Environmental Research Center Papers

Number 2

1983

Environmental Research Center
The University of Tsukuba

EXPERIMENTS ON BEDLOAD TRANSPORT, BED FORMS, AND SEDIMENTARY STRUCTURES USING FINE GRAVEL IN THE 4-METER-WIDE FLUME

By Hiroshi Ikeda

Environmental Research Center, the University of Tsukuba
Ibaraki, 305 Japan
(received December 17, 1982)

ABSTRACT

Four cases of experiments, using fine gravel, on sediment transport, were carried out in the 4-meter-wide flume, at the University of Tsukuba. For Cases 1 to 3, each slope was established at 1/100, 1/200, and 1/400, respectively. The change in flow and bed conditions with an increase in discharge, was investigated. In Case 4, the bar development process on a planed bed with a slope of 1/100, was investigated.

In this paper, the experimental results for each case were described separately, and the following points were confirmed. When the stream power and the depth of flow/grain size of bed material ratio are kept constant, in a flow with a little stream power, the larger the slope is, the higher the bedload transport rate becomes. The reason for this is that, the larger the slope, the smaller the threshold stream power, and thus, oppositely, the greater the amount of available power for bedload transport.

Secondly, the exponent in the relationship between the bedload transport rate and the available stream power at a high transport stage is 3/2, when the depth is kept constant. However, if the discharge is changed but the slope is kept constant, this value approches 1, and if the slope is changed but the discharge is kept constant, it approaches 2. Furthermore, at the same stream power, the steeper the slope and the shallower the depth, the higher the bedload transport rate. However, by simply increasing the flume width and decreasing the depth at the same stream power, without changing the slope, the bedload transport rate will instead become lower.

Thirdly, it was confirmed that there is a relationship between, the angle between the oblique crests formed on a planed bed and the flume side walls, (β), and the spacing of longitudinal striations (L_l) and the wavelength of antidunes (L_t), which can be described by, $\beta = \tan^{-1} \frac{L_l}{L_t}$. Hence, it was suspected that rhomboidal bars with oblique crests are formed by the interaction of longitudinal and transverse elements within the flow.

Using the alternating bars formed in the 4-meter-wide flume as the prototype, model rules were examined using a flume 1/20th its width. As a result, it was confirmed that, by making the values of the flow intensity (U_*/U_{*c}) and the channel form index ($S \cdot W/D$) equivalent to those of the prototype, the bar-bed configuration of the model would become similar to that of the prototype.

From the reults of the small flume experiments on the transport of the sand and gravel mixture, it was found that, no matter how strong the water flow, not all of the sand in the bed material is suspended, and thus openwork gravel layers (i. e., gravel layers without matrices)

never occur. In fact, it was made apparent that, in the formation of bed forms, the complete segregation of sand and gravel takes place on river beds, because the bed material is sorted into groups of different grain sizes.

CONTENTS

LIST OF FIGURES

Figure

LIST OF TABLES

LIST OF SYMBOLS

A	area of flow cross section
C_s	sediment concentration of sand fraction
C_t	total sediment discharge concentration
d_m	mean size of bed material
d_{50}	median size of bed material
D	depth of flow
F	Froude number = $V/\sqrt{gD}$
g	acceleration due to gravity
i_b	bedload transport rate per unit width of flume (immersed weight)
I_b	bedload transport rate per total flume width (immersed weight)
L	length of flume
	scale of horizontal direction
L_b	bedload transport rate per total flume width
L_l	spacing of longitudinal striations
L_t	wavelength of antidunes
M	weight percent of sand in bed material
q	water discharge in volume per unit width per unit time
Q	water discharge in volume per unit time
S	water surface slope
S_o	graphical measure for sorting = $(\phi_{84} - \phi_{16})/2$
T	time
	total duration of run
T_w	water temperature
U_*	$=\sqrt{gDS}$ shear velocity
U_{*c}	critical value of U_* for initiation of sediment motion
V	$= Q/W \cdot D$ mean velocity of fluid
V_b	velocity of alternating bars
V_s	surface velocity of fluid
W	width of flume
X_m	subscript m signifies the values of the model
X_p	subscript p signifies the value of the prototype
X_r	$= X_p/X_m$ subscript r signifies the ratio of the prototype to the model
Y	scale of vertical direction
β	angle between oblique crests of rhomboid bars and flume side walls
λ	wavelength of alternating bars
ρ	density of fluid
σ	density of bed material
ϕ	$= -\log_2 d$ phi scale (where d is the diameter of particle in millimeters)
ω	stream power per unit bed area = $\rho gVDS$
Ω	stream power per unit length of flume = ρgQS

ω_0 threshold value of ω for bedload transport

Ω_0 threshold value of Ω for bedload transport

CHAPTER 1

INTRODUCTION

Recently, in hopes of maintaining a comfortable and safe society, the quantitative prediction of landform evolution is desired. For this reason, there is a rising necessity to clearly understand the mechanism of topographic change due to fluvial processes. Many flume experiments were done on the transport and deposition of sediments in alluvial rivers since the 19th century (Graf, 1971). However, geomorphic processes operating in natural alluvial channels were not clearly understood, and what is more, most flumes used previously had been small and all had certain weaknesses. Thus, there were still a great many unsolved problems associated with the transport and the deposition of sediments in alluvial rivers (Vanoni, 1975).

At the time of the construction of the flume in the Environmental Research Center at the University of Tsukuba, the following considerations were made:

to reduce the side wall friction of the flume to a minimum

to have the flow in the flume sufficiently deep so that the turbulence can be examined

to simulate variations in the textural proportions of bed material in natural rivers

to conduct long-period experiments without interrupting the sediment or the water supply

The resultant flume is 4m wide, 2m deep, and 160m long. Since 1975, I have participated in the planning and construction of the flumes, as a staff member of the Environmental Research Center. We studied thoroughly the results of researches on sediment transport by Bagnold (1960, 1966, 1973, 1977), after having been recommended by Dr. Masao Inokuchi, the former directer of the Environmental Research Center.

In August 1978, when the flume was nearly completed except for part of the equipment, the travel velocities of particles of various sizes and densities rolling on a smooth bed, were examined at different flow depths (Ikeda, et al. 1979).

Results showed that the relative or slip velocity of particles (i.e., the difference between the speed of the fluid and that of the particle), is not equal to the fall velocity of the particle in still water, but rather, is proportional to the intensity of the viscous resistance on the particle. This viscous resistance is caused by the particle's revolution in the viscous fluid.

In May 1979, actual experiments on the sediment transport of fine gravel with diameters between 5–10mm, were begun. Uniform, fine gravel was used for bed material for the following reasons:

1. micro-scale bed forms, such as ripples are not formed,
2. the sediment is transported as bedload,
3. fine gravel was not often used in previous experiments, hence there was relatively little data, and
4. no problems or difficulties arise in the sediment recirculation system.

The experimental results of the bedload transport experiments obtained between May 1979 and July 1980, were presented at the 24th International Geographical Congress, which was held in Tokyo, September 1980 (Ikeda, 1980). Since then, investigations on bar developments on planed beds were made, between September 1980 and May 1981.

In this paper, the results of the experiment using fine gravel are described and the following four points are discussed:

1. the relationship between the bedload transport rate and the stream power,
2. the origin of rhomboid bars,
3. the similitude law (or model rules) of alternating bars, and
4. conditions for the formation of openwork gravel layers.

CHAPTER 2

EXPERIMENTAL PROCEDURES

2-1 Equipment used

The flumes and related equipment used in this experiment are in the Environmental Research Center at the University of Tsukuba (Fig. 2-1).

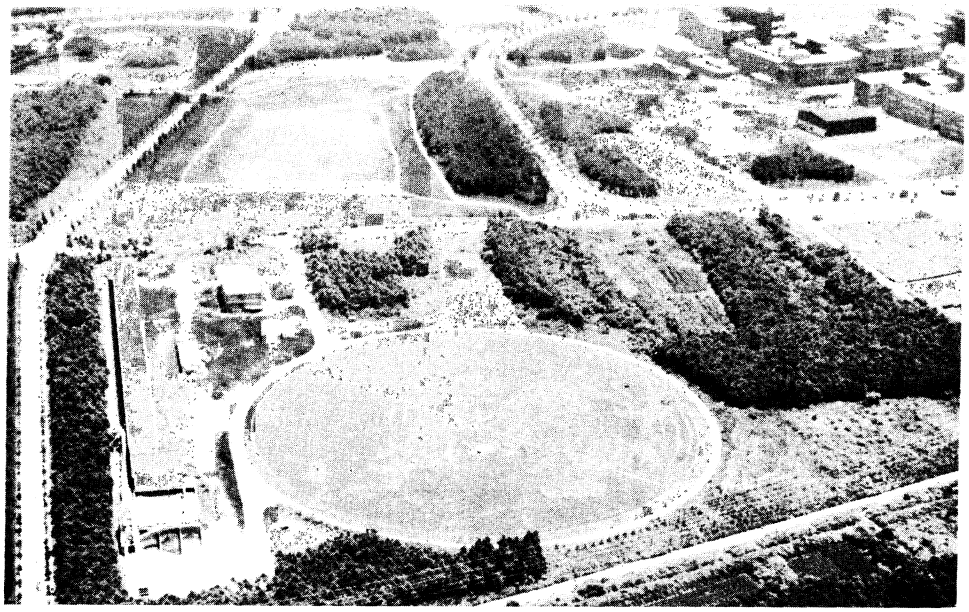

Fig. 2-1 Aerial view of the Environmental Research Center

Most of the data were collected in a recirculating steel flume, 4 meters wide, 2 meters deep, and 160 meters long. It is completely housed, and was constructed during 1976–1979 (Fig. 2-2). The flow may be varied from 0 to 1.5 m^3/sec by the use of three pumps, and is regulated by the operation of an overflow gate in the high water tank. The inclination of the flume was fixed at a slope of 1/100. However, the inclination of the stream bed may be varied from 0 to 1/50 through the operation of a gate system at the foot of the flume.

The flume can be operated by either a sediment recirculating system or a feed system. In the recirculating system, sediment that has been deposited in the settling tank installed at the outlet of the flume is recovered, and after weighing transported back by a converyor belt to the head of the flume, where it is fed again into the flume. On the other hand, in the feed system, the recovered sediment is transported by a conveyor belt to sieving and mixing equipment, and after the adjustment of grain size, it is fed into the flume. Detailed descriptions on the structures of the flume have been given by Inokuchi, et al. (1980).

▼Observation carriage
Electric carriage equipped with a transverse capability in order to measure flow velocity, water depth, and the height of the sand bed

▼ Control room
Equipped with an operation table for remote control of the various flume devices and with controls for the monitoring television and data gathering system

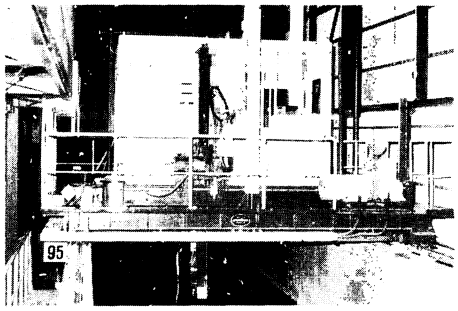

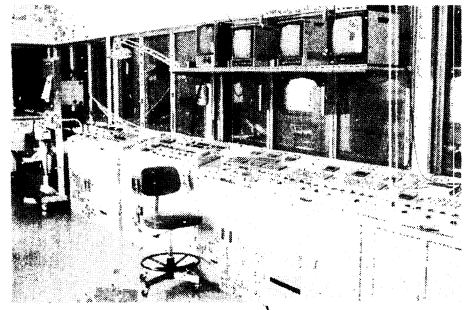

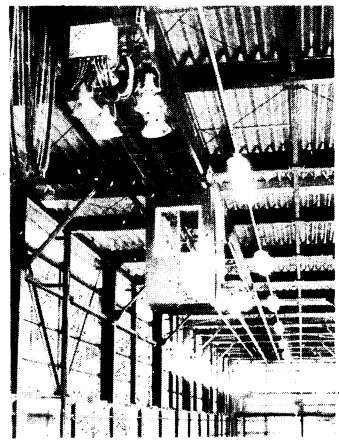

Photographic carriage ▲
Electric carriage suspended from the roof and running automatically with a variable speed (0 - 1 m/sec) allows stereo photography of flow and bed features

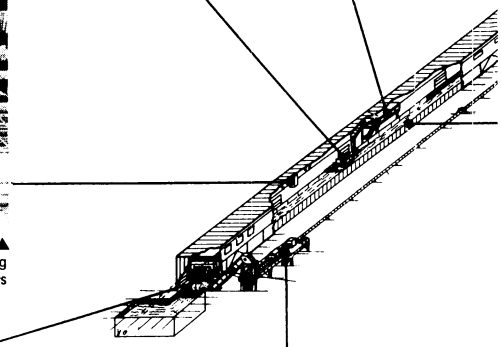

◀ Sediment recovery device
Belt conveyor system for the recovery of sediment deposited in the settling tank at the foot of the flume

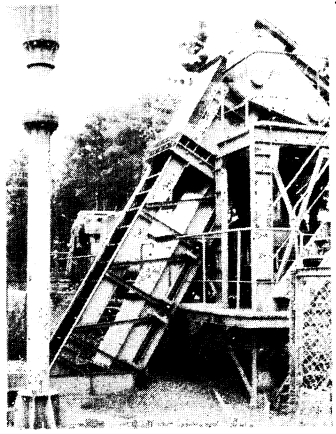

Sediment weigher and sediment ▶ recirculation conveyor

Fig. 2-2 The 4-meter-wide flume

▼ **Pumping equipment**
Three pumps of 500 mm diameter are used to supply a maximum discharge of 1.5 t/sec.
The discharge is regulated by the operation of a gate in the high water tank

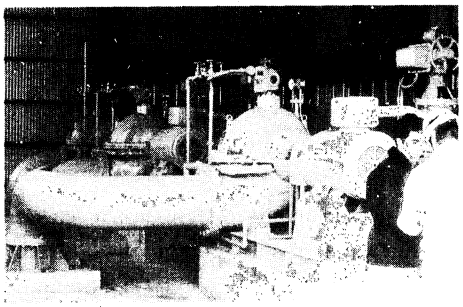

▼ **Water reservoir**
Stocks as much as 2,000 m^3 of water which is returned from the foot of the flume through an underground piping system

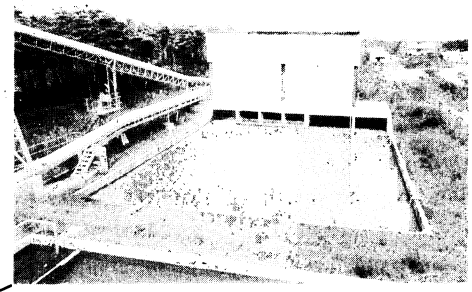

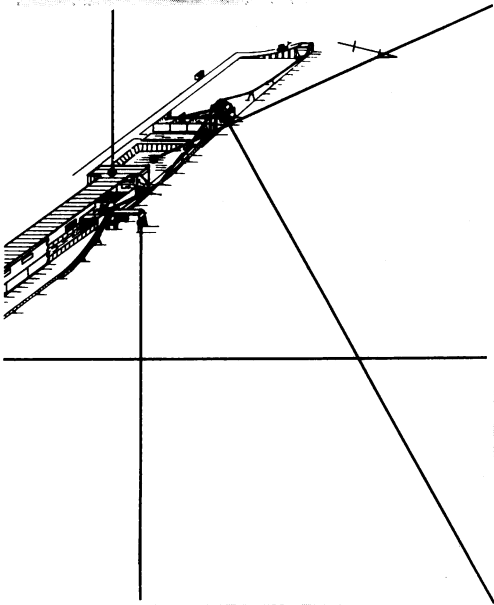

▲ **Flume**
Steel flume that is 4 m wide, 2 m deep, and 160 m long. Its fixed inclination is 1/100. However, the gradient of the stream bed is variable through the operation of a gate system at the foot of the flume

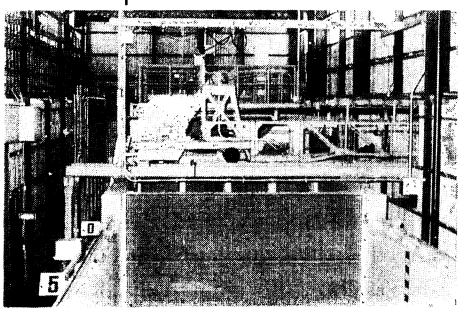

▲ **Sediment feeder**
Conveyor system for feeding sediment to the flume

▲ **Sieving and mixing system**
Automatic sieving system for sediment from 0 - 20 mm in diameter. Sediment can be sorted into three sizes and mixed to desired ratios

2-2 Measurements of variables and parameters

The following variables were measured:

a) Water surface slope, b) Depth of flow, c) Water discharge, d) Water temperature, e) Bed material discharge, f) Size gradation of sediment, g) Bed configuration.

a) Water surface slope

In the experiment, the electric water-level meter continuously recorded the elevation of the water surface at six points along the flume. Thus the water surface slope was determined automatically from the data.

b) Depth of flow

The average depth of flow was determined by measuring the differences in elevation between the water-surface and the gravel bed surface across the flume with an electric depth gauge attached to the observation carriage.

Measurements of flow depths were made at pre-selected intervals down the length of the flume. However, when the flow presented a braided pattern and sand banks appeared above water surface, no further reliable data for the depth of flow could be taken.

c) Water discharge

Water discharge was regulated by the operation of a gate in the high water tank. Thus, water discharge was determined by measuring the elevation of water surface over the triangular weir in the head tank with an electric water-level meter.

d) Water temperature

Water temperature was continuously measured in the return-flow lines with a calibrated thermocouple.

e) Bed material discharge

Sediment that has been carried out from the flume and deposited in the settling tank is continuously recovered, and is weighed by a sediment weigher in the sediment recirculation conveyor. Water content of the sediment on the conveyor belt is always nearly 5% by weight. For runs having a relatively low rate of sediment discharge, in order to keep the accuracy of weighing, recovered sediment is accumulated in a hopper and weighed periodically.

f) Size gradation of sediment

Samples of the bed material carried out from the flume were taken by scooping from that on the conveyor belt for size analysis. The median particle size and the gradation distribution of some samples were determined in terms of sieve diameter.

g) Bed configuration

The general bed configuration was noted visually and was also recorded photographically. Observation was made at the end of the run, after the water had been carefully drained out, if the water was not clear and the depth was large. For some runs, longitudinal profiles of the bed configurations were obtained with a sand-level gauge.

Several of these measured variables can be used to compute other variables and parameters useful for evaluating flow and transport characteristics in the flume channel. These variables include:

1. Mean velocity, 2. Shear velocity, 3. Stream power, 4. Reynolds number, 5. Froude number, 6. Resistance factors.

2-3 Operation procedures

Runs were made in four cases, from Case 1 to Case 4, with fine gravel in the 4-meter-wide flume. The sediment used as bed material was artificially sorted into a nearly uniform fine gravel. A particle-size distribution curve (size in millimeters vs. percentage finer than indicated size) is shown in Fig. 2-3. Fig. 2-4 is a photograph of the sediment to show its roundness and gradation. The specific gravity of the sediment is 2.65.

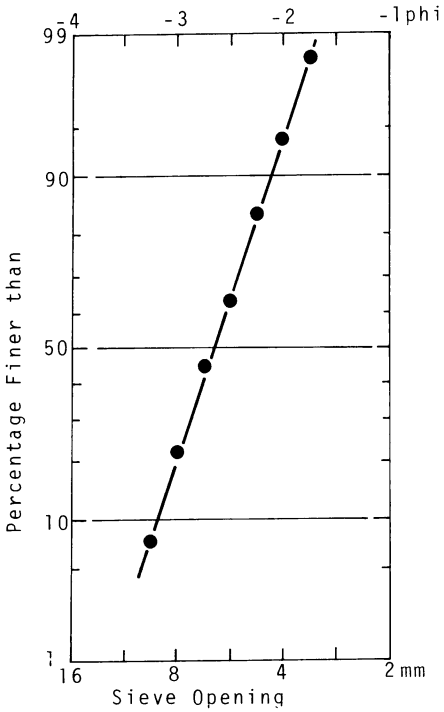

Fig. 2-3 Particle size distribution curve for bed material

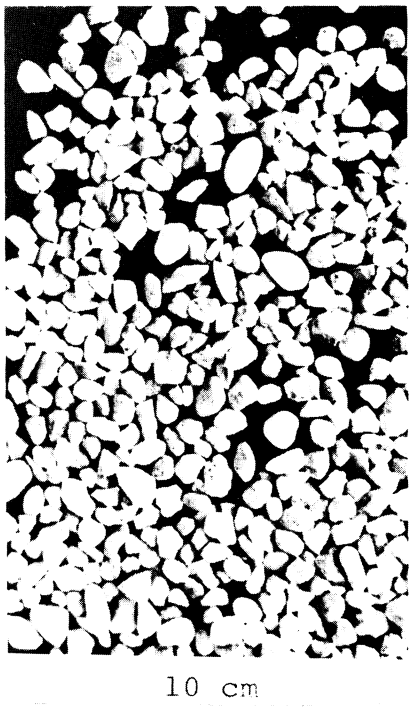

Fig. 2-4 Fine gravel used for the experiments

Cases 1, 2, and 3 were made between May 1979 and July 1980. The purpose of these cases was to observe the sequential changes in the bed configurations formed in a laboratory flume, and to obtain data for the bed material transport rate by progressively increasing the discharge up to 1.5 m^3/sec, when fine gravel was used as bed material.

Pre-set slopes of Cases 1, 2, and 3 were 1/100, 1/200, and 1/400, respectively. Depth/grain size ratio ranged between 10 and 50. In each case, the bed was not planed before each run. Experimental variables and parameters for Cases 1 to 3 are given in Table 2-1.

Case 4 was made between September 1980 and May 1981. The purpose of Case 4 was to observe the development of bars from a flat bed at different depth. The general procedure was different for the runs in this case. Before each run, the desired preset slope of 1/100 was established by planing the bed.

Table 2-1 Summary of experimental data for Cases 1 to 3

Run No.	Q m^3/sec	T_w °C	S $X10^{-2}$	D m	V_s m/sec	Bed state	L_b kg/sec	I_b kg/sec	Ω kg/sec
Case 1									
58	0.075	26.1	0.969	–	–	A	a0.0061	0.0038	0.724
57-2	0.088	26.6	0.914	–	–	A	a0.0032	0.0020	0.802
57	0.090	25.5	0.970	–	–	A	a0.0013	0.00082	0.870
56	0.115	23.5	0.958	–	–	A	a0.049	0.031	1.10
7	0.122	20.1	0.977	–	–	A	a0.026	0.017	1.19
12	0.125	20.2	0.922	–	–	A	a0.044	0.028	1.15
11	0.145	21.0	0.938	–	–	A	0.075	0.047	1.36
55	0.147	22.5	0.961	–	–	A	a0.074	0.060	1.41
1	0.155	16.6	0.984	–	–	A	0.175	0.110	1.53
13	0.175	20.9	0.948	–	–	A	a0.100	0.063	1.66
54	0.200	23.1	0.972	–	–	A	0.142	0.089	1.94
5	0.235	19.3	0.981	–	–	A	0.284	0.179	2.31
14	0.245	21.1	0.975	–	–	A	0.367	0.231	2.39
10	0.285	21.0	0.974	–	1.10	A	0.442	0.278	2.78
2	0.345	19.0	0.961	–	–	A	0.672	0.423	3.32
15	0.358	23.3	0.962	0.084	1.23	A ~ B	0.648	0.408	3.44
16	0.500	24.3	0.948	0.120	1.30	C	1.06	0.667	4.74
3	0.500	19.0	0.968	–	–	C	1.25	0.787	4.84
6	0.690	20.0	0.980	–	–	C	1.88	1.18	6.76
17	0.730	24.4	0.981	–	–	C	1.88	1.18	7.16
4	0.980	19.0	0.982	–	–	E	3.00	1.89	9.62
53	1.04	23.6	0.982	–	–	E	2.69	1.70	10.2
18	1.05	25.1	0.997	0.178	1.75	E	3.00	1.89	10.5
9	1.18	21.0	0.974	–	–	E	3.83	2.41	11.5
8	1.39	21.0	0.985	–	–	E	5.01	3.15	13.7
19	1.47	25.0	0.975	0.246	1.75	E	4.38	2.76	14.3
4-7	0.413	10.5	1.02	–	–	C	0.787	0.496	4.21
4-8	0.506	11.0	1.08	–	–	C	1.14	0.719	5.46
4-9	0.302	11.5	1.03	–	–	A ~ B	0.461	0.290	3.11
4-10	0.803	12.0	1.07	–	–	C	2.10	1.32	8.59
Case 2									
52	0.150	24.7	0.480	–	–	A	a0.00028	0.00017	0.722
51	0.180	23.6	0.491	–	–	A	a0.0016	0.00099	0.881
50	0.216	23.7	0.485	–	–	A	a0.020	0.013	1.04
49	0.262	23.0	0.475	–	–	B	a0.025	0.016	1.24
24	0.356	25.5	0.485	0.135	1.07	B	0.066	0.042	1.73
25	0.500	25.7	0.515	0.159	1.14	B	0.308	0.194	2.57
26	0.710	25.1	0.472	0.179	1.36	C	0.517	0.326	3.35
46	0.944	20.6	0.509	–	–	C	0.764	0.481	4.80
27	1.01	24.2	0.494	0.198	1.52	E	1.01	0.634	4.99
20	1.04	26.0	0.544	0.219	1.37	E	0.978	0.616	5.66
Case 3									
44	0522	22.0	0.218	–	–	B	a0.000097	0.000061	1.14
38	0.522	24.0	0.247	0.154	0.99	B	a0.0010	0.00064	1.29
42	0.600	–	0.213	–	–	B	a0.00063	0.00039	1.27
37	0.622	24.0	0.250	0.171	1.06	B	a0.0061	0.0038	1.56
43	0.705	22.8	0.221	–	–	B	a0.0099	0.0062	1.55
32	0.714	23.5	0.228	0.186	1.05	B	a0.015	0.0092	1.63
36	0.744	23.5	0.241	0.189	1.08	B	a0.012	0.0076	1.79
41	0.802	23.2	0.228	–	–	B	a0.027	0.017	1.82
33	0.856	23.0	0.248	0.211	1.17	B	0.134	0.084	2.12
45	0.927	21.5	0.240	–	–	D	0.131	0.083	2.21
29	0.980	22.7	0.254	0.248	1.21	D	0.183	0.115	2.49
40	1.11	24.0	0.255	–	–	D	0.196	0.123	2.82
34	1.24	24.2	0.261	0.278	1.33	D	0.374	0.235	3.24
35	1.54	24.3	0.269	0.313	1.37	D	0.669	0.421	4.14

Bed state:

A, multiple-row bars; B, alternating bars; C, alternating bars with standing waves; D, low relief dunes; E, antidunes

[a] L_b: measured with hopper; –: not measured

CHAPTER 3

EXPERIMENTAL RESULTS

3-1 Changes in the flow and bed conditions with increasing discharge at a slope of 1/100 (Case 1)

Changes in the flow conditions and bed configurations caused by progressively increasing the discharge at a fixed slope of 1/100 are as follows (See Fig. 3-1).

In the runs with low discharge the moving bed forms were small scale multiple row bars, which caused the flow to braid (Figs. 3-2 and 3-3). The individual bars changed shape with time and moved very slowly. With gradually increased discharge, the bed configurations changed from multiple row bars to alternate bars (Fig. 3-4). Alternate bars (Fig. 3-5) caused the flow to meander. It was observed that trains of standing waves formed on the back of alternate bars, and that occasionally a wave would break gently (Fig. 3-6).

In these runs, the rate of sediment discharge deposited in the settling tank at the foot of the flume showed rhythmic changes, in spite of the equilibrium condition achieved (Fig. 3-7). These changes are due to the migration of bars in the flume. Therefore, it is necessary to have continuous experiments over a long period enough to obtain reliable sediment transport data.

Increasing the discharge caused more antidune activity to occur (Fig. 3-9), and standing waves formed from wall to wall across the flume at approximately right angles to the flow (Figs. 3-10 and 3-11).

3-2 Changes in the flow and bed conditions with increasing discharge at a slope of 1/200 (Case 2)

In each run in Case 2, the slope was kept constant at 1/200 by adjusting the tail gate. Fig. 3-13 shows the bed configurations in Case 2. Measured changes of sediment discharge for some runs are shown in Fig. 3-14.

Little changes in bed configurations occured if the discharge of the runs was less than 0.25 m^3/sec. Alternate bars developed for runs with discharge between 0.25 and 0.5 m^3/sec (Figs. 3-15 and 3-16). Their length was approximately 5.5 times the flume width. When the discharge was more than 0.5 m^3/sec, the length of the alternate bars increased to about 9 times the flume width (See Figs. 3-13 and 3-17). By further increaseing the discharge to 1 m^3/sec, the bed form changed from long alternate bars to short diagonal bars (Fig. 3-18). Increased discharge caused the surface flow condition to become more turbulent, and it was observed that low relief antidunes or dunes were formed (Fig. 3-19).

3-3 Changes in the flow and bed conditions with increasing discharge at a slope of 1/400 (Case 3)

The preset slope for runs in Case 3 was 1/400, and Fig. 3-20 shows the configuration of this case. Measured changes in sediment discharge for some runs are shown in Fig. 3-21. When the discharge was between 0.5 and 1 m^3/sec, the length of the alternating bars was 7.5 to 10 times the flume width (See Fig. 3-20).

It was observed that the back of the bars were relatively smooth (Fig. 3-22). In these runs, the transport rate was very low, so that the migration velocity of the bars was extremely slow. When the discharge was more than 1 m^3/sec, increasing the discharge caused the bars to gradually

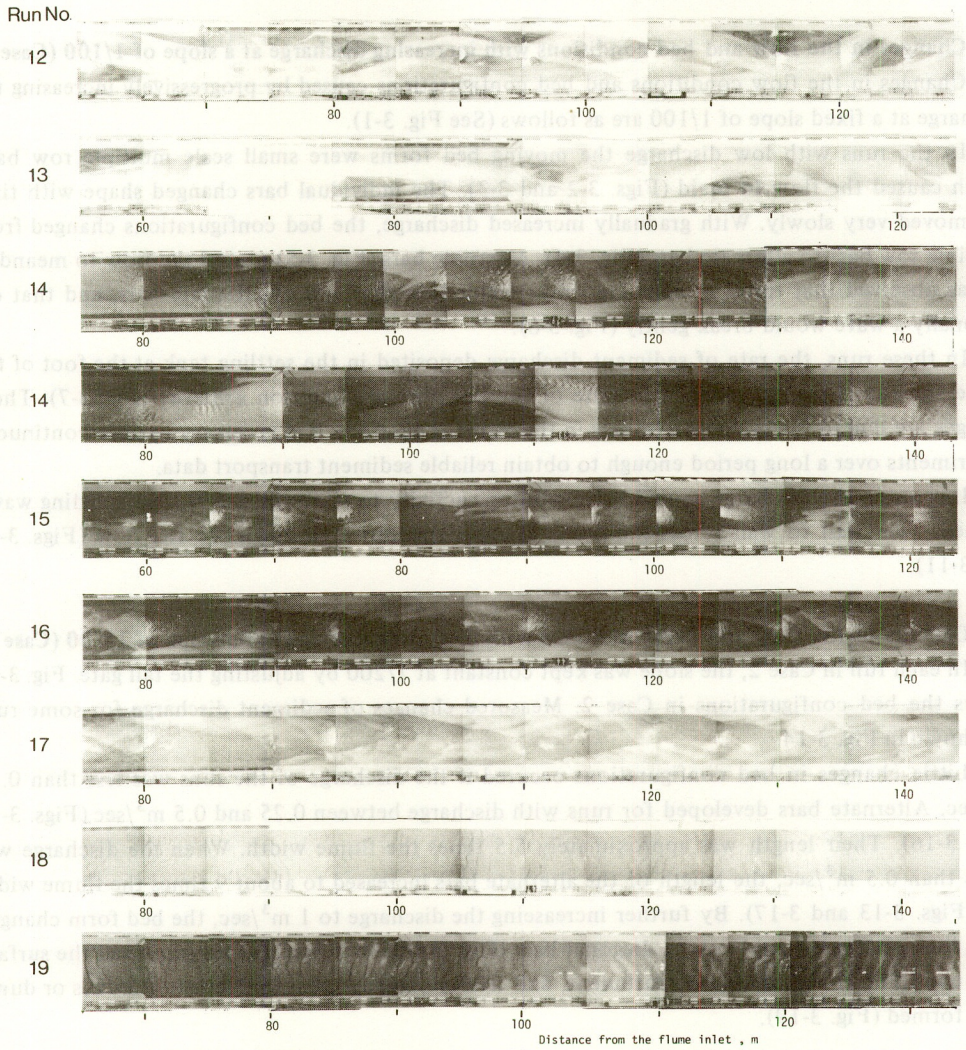

Fig. 3-1-1 Changes in the shape of bed configurations with increasing discharge at slope 1/100 (Case 1)

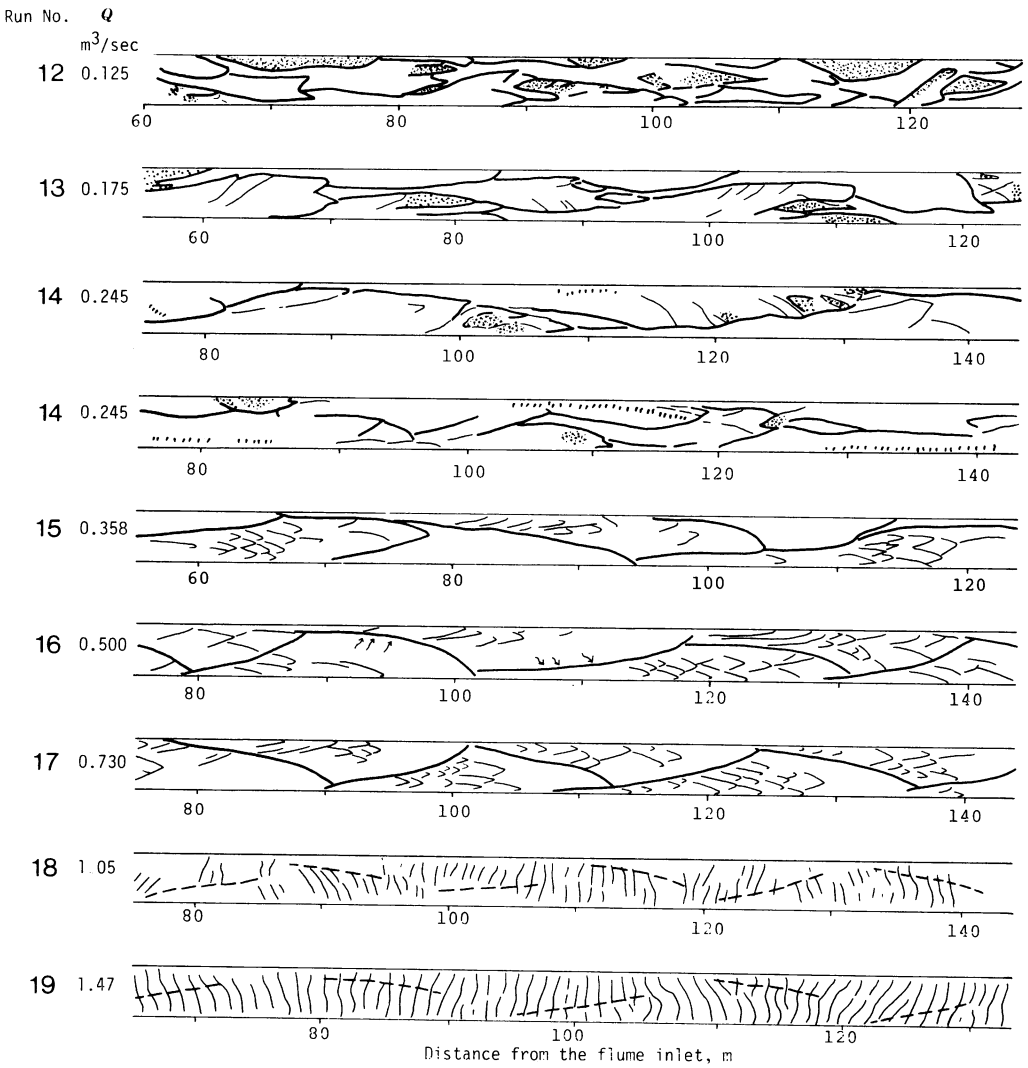

Fig. 3-1-2 Changes in the shape of bed configurations with increasing discharge at slope 1/100 (Case 1)

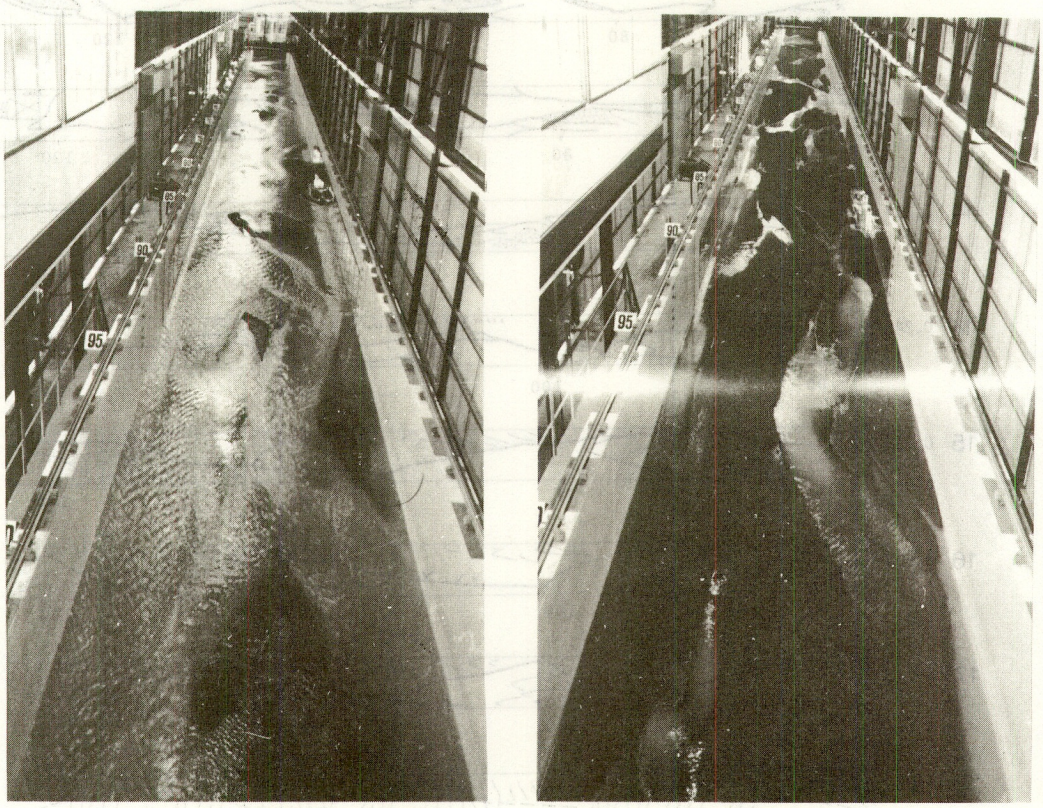

Fig. 3-2 Upstream views of bar-bed configuration for Run 12 (S = 1/100, Q = 0.13 m^3/sec)
(A) Water surface showing braided stream patterns
(B) Bed configuration at end of run

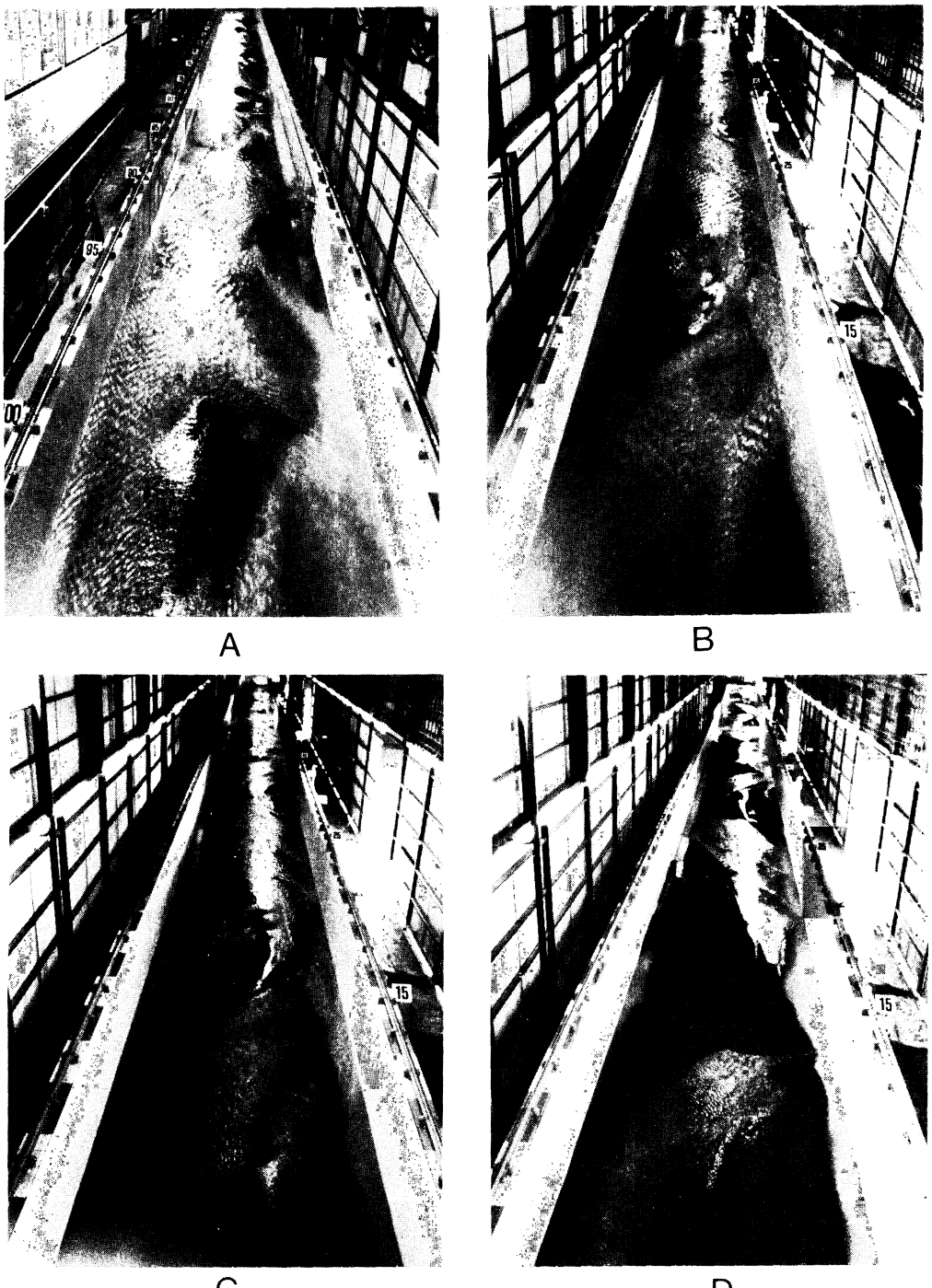

Fig. 3-3 Flow and bed conditions for Run 13 (S = 1/100, Q = 0.18 m^3/sec)
(A) Upstream view of water surface condition, showing braided stream patterns
(B) ~ (D) Downstream views of bed configurations as flow wanes

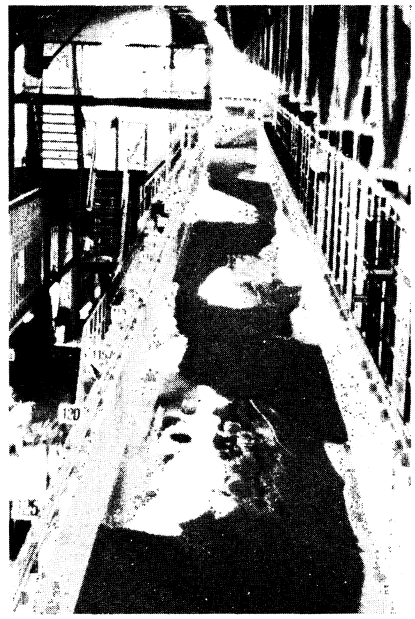

Fig. 3-4 Upstream view of bars formed during Run 15 (S = 1/100, Q = 0.36 m^3/sec)
The bed configuration is a transitional form of alternate bars and double row bars. The length of the bars is approximately 6 times the flume width.

Fig. 3-5 Upstream view of alternating bars for Run 16 (S = 1/100, Q = 0.50 m^3/sec)
The length of the bars is approximately 3 times the flume width. Bed material discharge fluctuated periodically for every 2 hours (Fig. 3-7). Therefore, the migration velocity of the bar was about 6 m/hour.

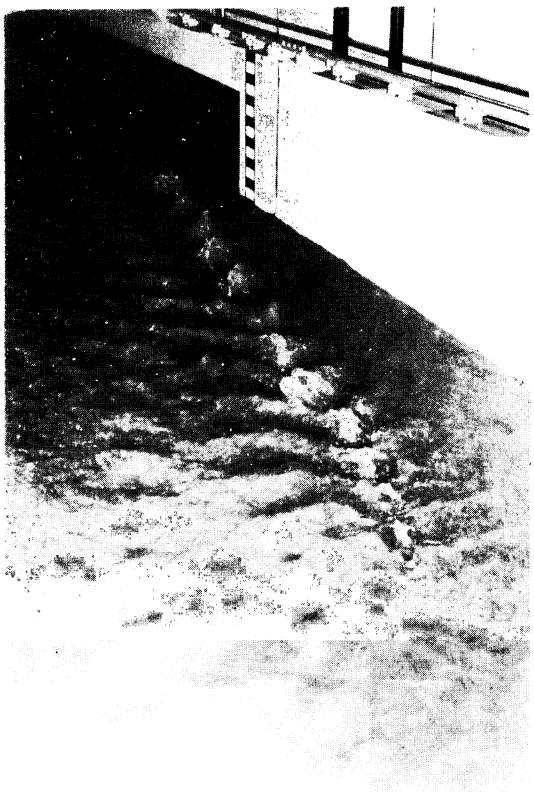

A

B

Fig. 3-6 Flow conditions for Run 16 (S = 1/100, Q = 0.50 m^3/sec)
(A) Trains of standing waves occurring on the back of each bar
The flow is toward the observer.
(B) Occasionally, a wave would breake gently
The flow is away from the observer.

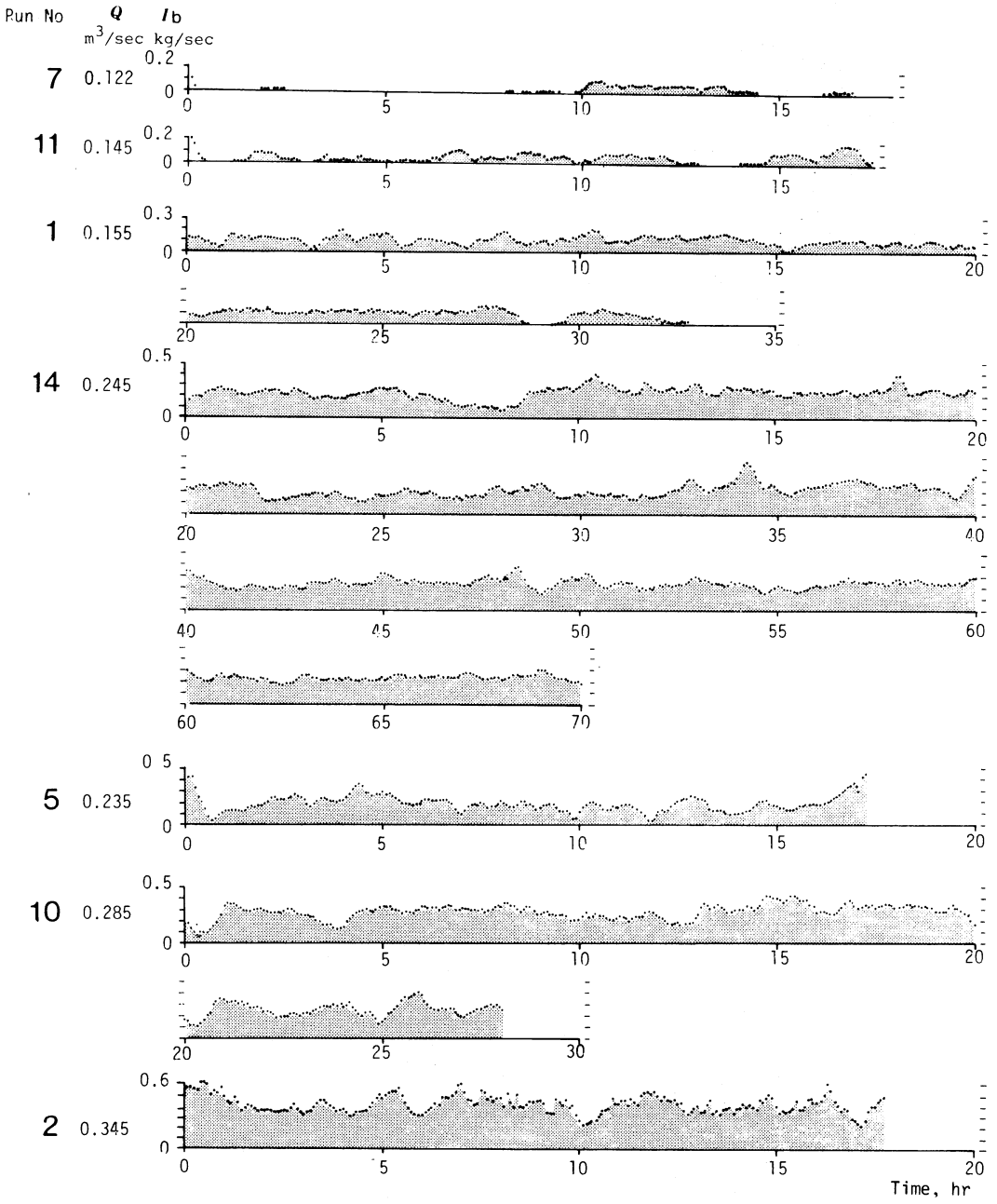

Fig. 3-7-1 Changes in bed material discharge at slope 1/100 (Case 1)

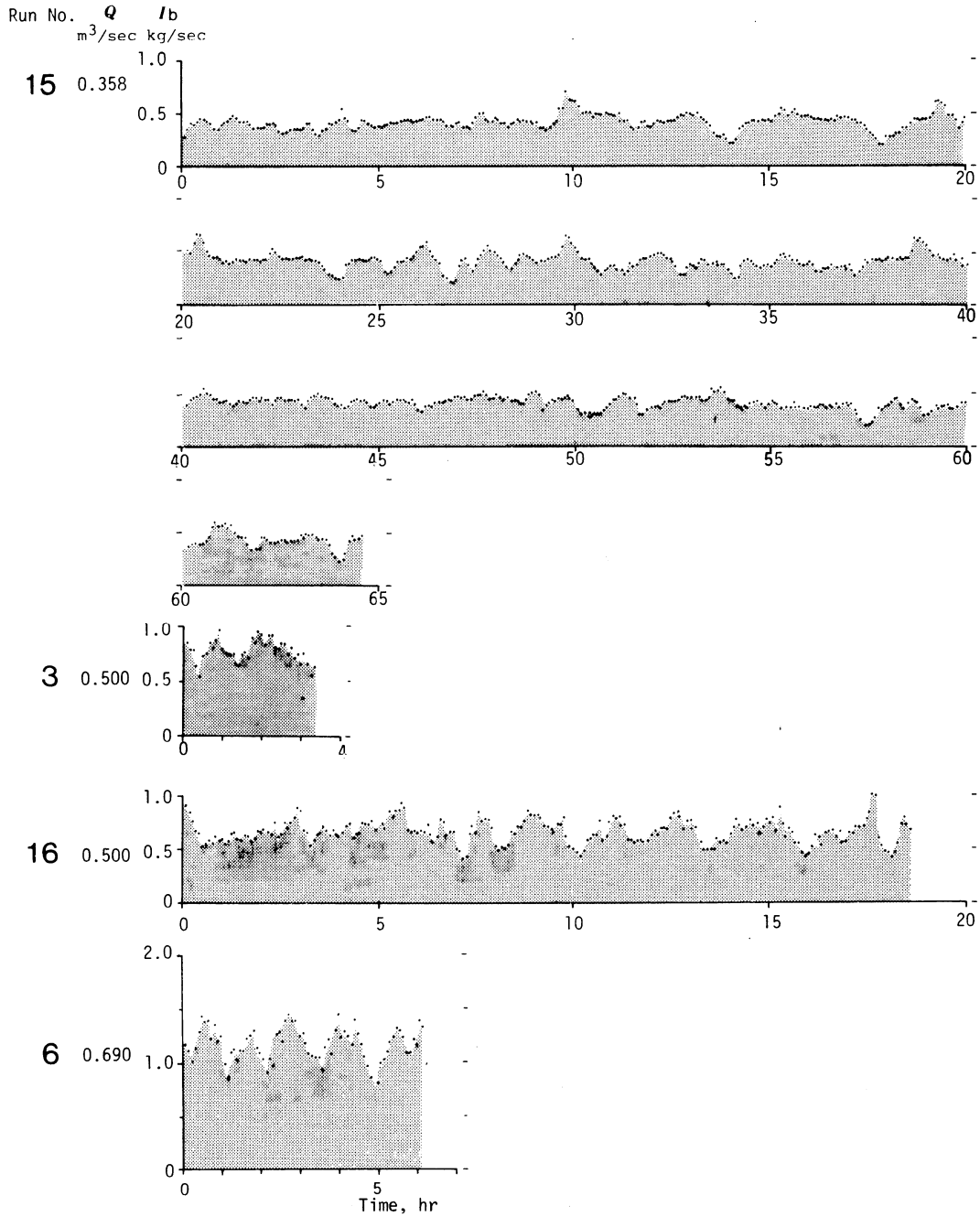

Fig. 3-7-2 Changes in bed material discharge at slope 1/100 (Case 1)

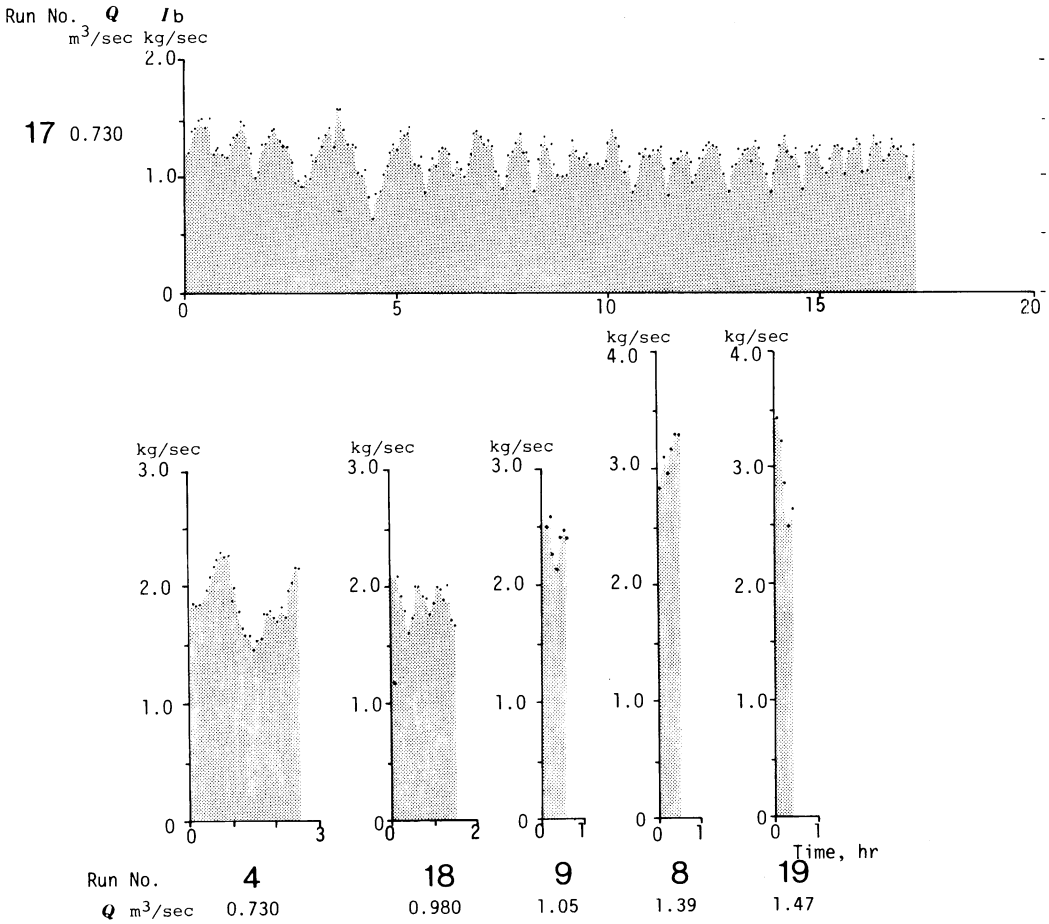

Fig. 3-7-3 Changes in bed material discharge at slope 1/100 (Case 1)
Each plotted point indicates the average value for every 5 minutes.

Fig. 3-8 Downstream view of typical alternating bars for Run 17 (S = 1/100, Q = 0.73 m^3/sec) Bed material discharge fluctuated periodically for every 50 minutes (Fig. 3-7). The length of bars is approximately 11 meters (Fig. 3-1). It shows that the migration velocity of the bar is approximately 13 m/hr.

Fig. 3-9 Upstream view of bed configurations at end of Run 18 (S = 1/100, Q = 1.05 m^3/sec)

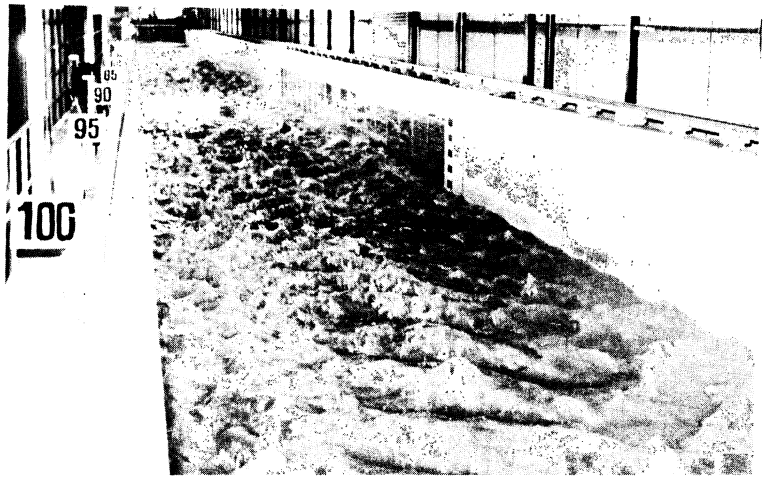

Fig. 3-10 Upstream view of choppy water surface for Run 9 (S = 1/100, Q = 1.2 m^3/sec)

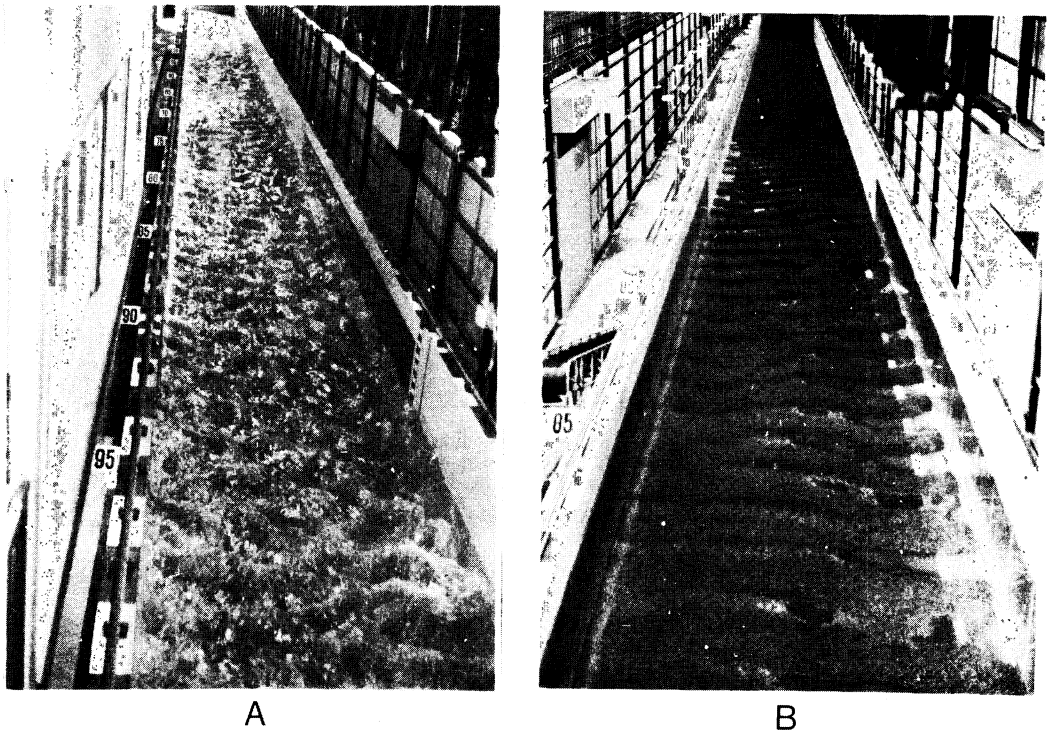

Fig. 3-11 Upstream views of flow and bed conditions for Run 19 (S = 1/100, Q = 1.5 m³/sec)
(A) Trains of standing waves and breaking waves extending from wall to wall in flume
(B) Increasing the water discharge causing more antidune activity to occur

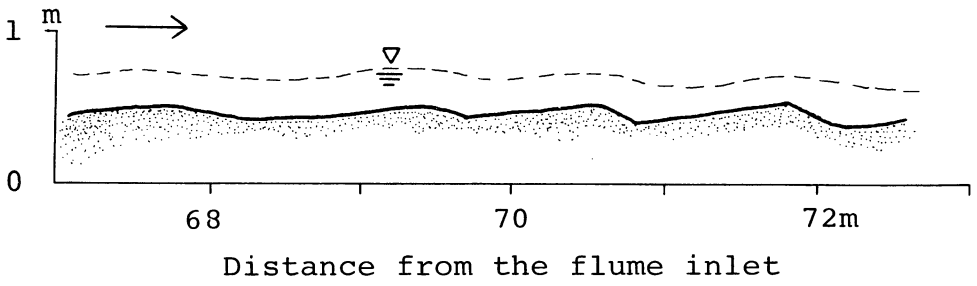

Fig. 3-12 Bed profile of antidunes for Run 19 (S = 1/100, Q = 1.5 m³/sec)

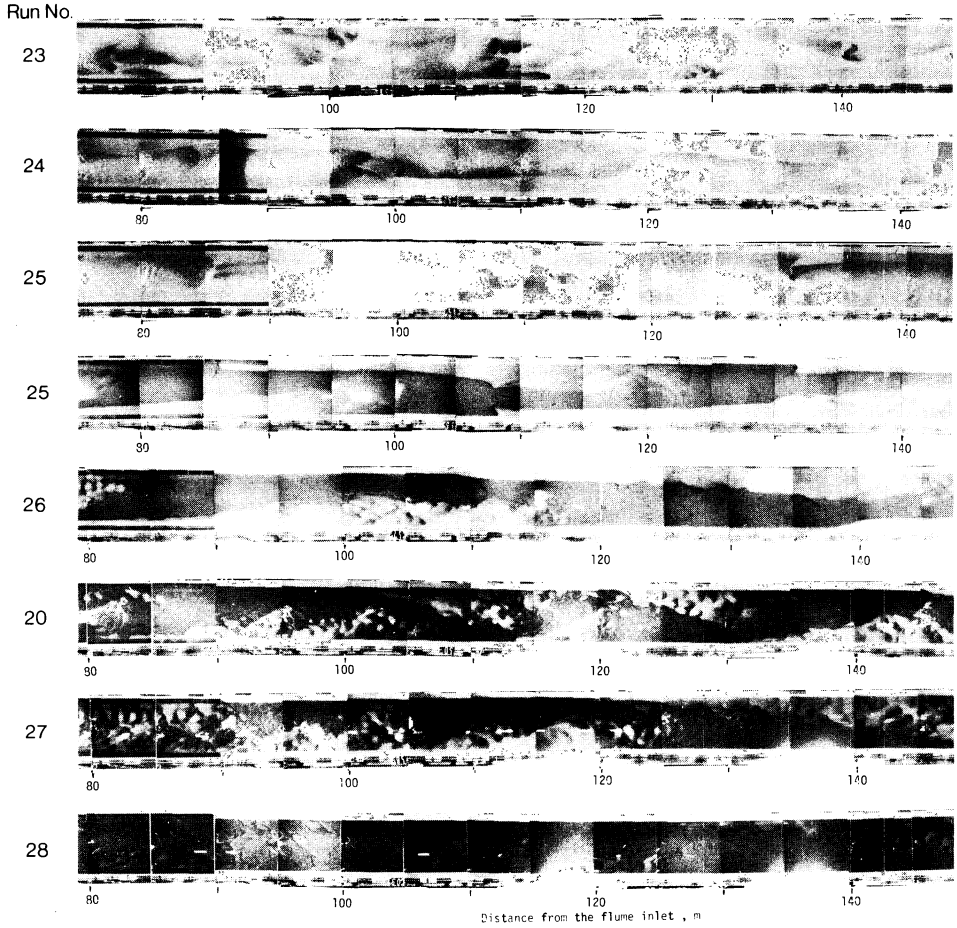

Fig. 3-13-1 Changes in the shape of bed configurations with increasing discharge at slope 1/200 (Case 2)

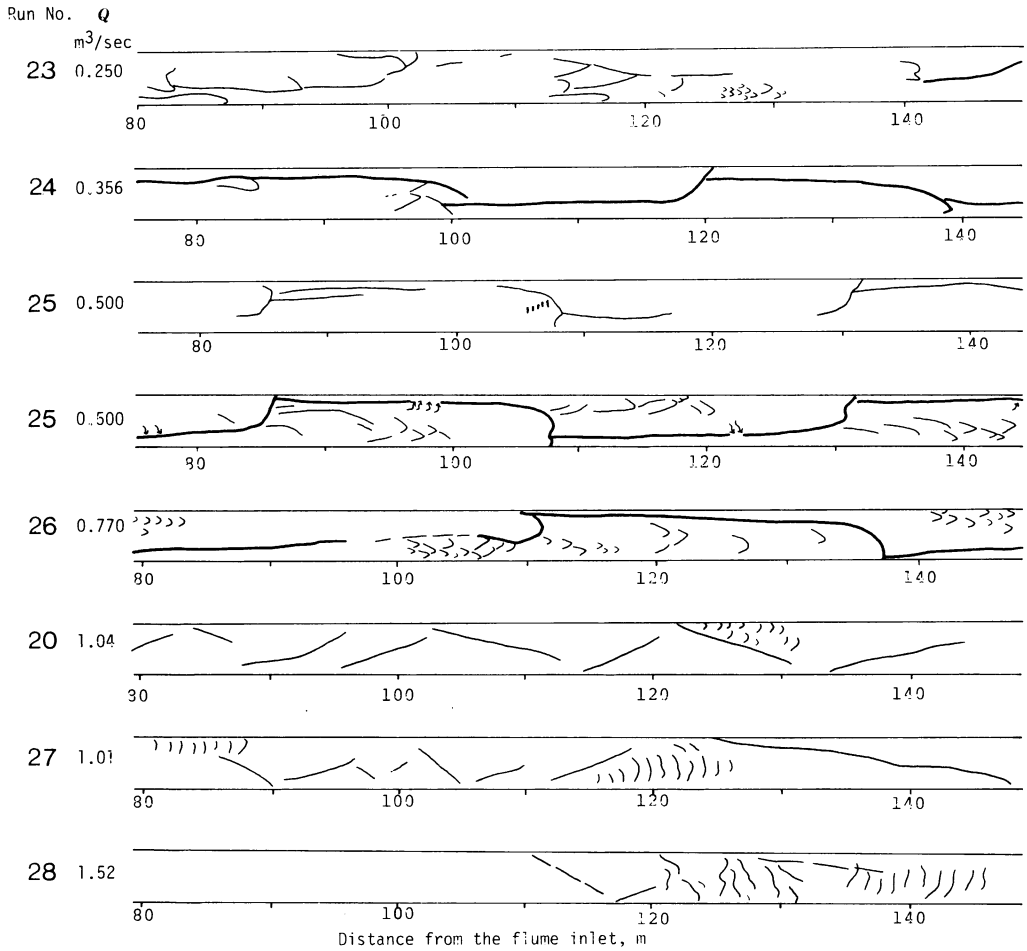

Fig. 3-13-2 Changes in the shape of bed configurations with increasing discharge at slope 1/200 (Case 2)

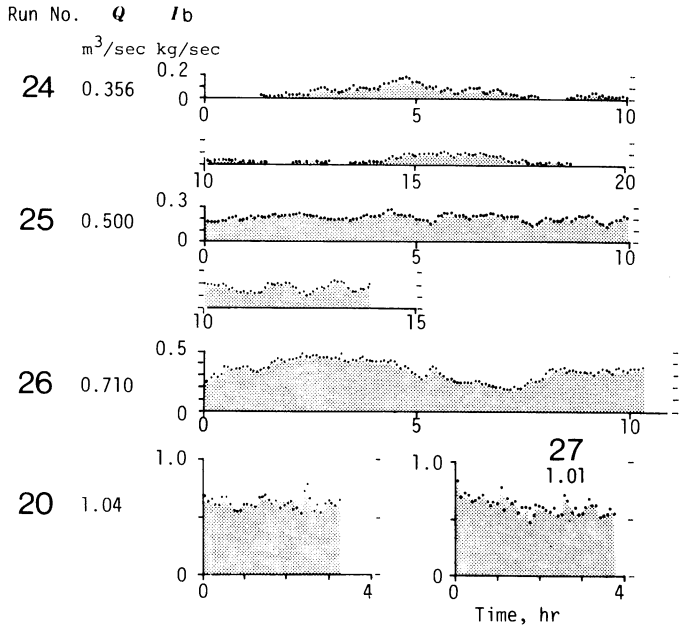

Fig. 3-14 Changes in bed material discharge at slope 1/200 (Case 2)
Each plotted point indicates the average value for every 5 minutes.

A B

Fig. 3-15 Flow and bed conditions for Run 24 (S = 1/200, Q = 0.36 m³/sec)
(A) Upstream view of surface flow condition.
The water surface is relatively smooth.
(B) Downstream view of alternating bars at end of run

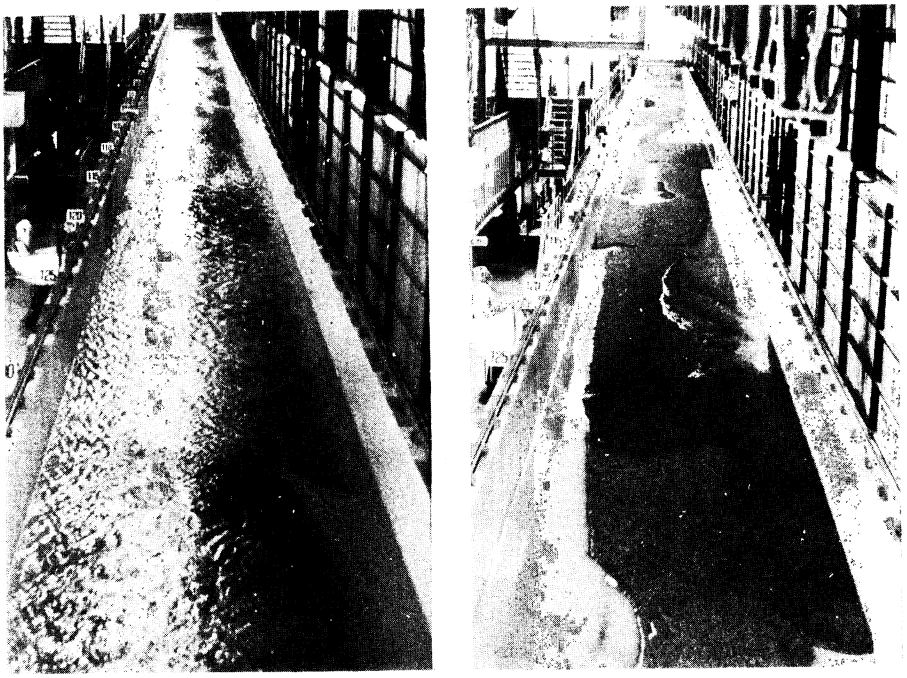

Fig. 3-16 Upstream views of flow and bed conditions for Run 25 (S = 1/200, Q = 0.50 m^3/sec)
(A) Surface flow condition
(B) Alternating bars at end of run

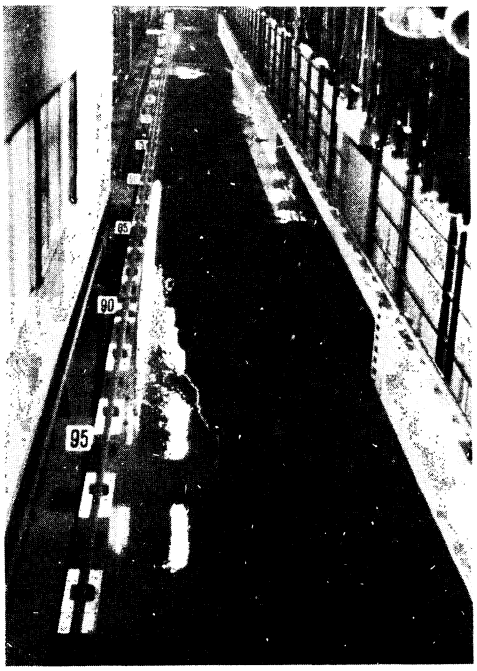

Fig. 3-17 Upstream view of alternating bars at end of Run 26 (S = 1/200, Q = 0.77 m^3/sec)

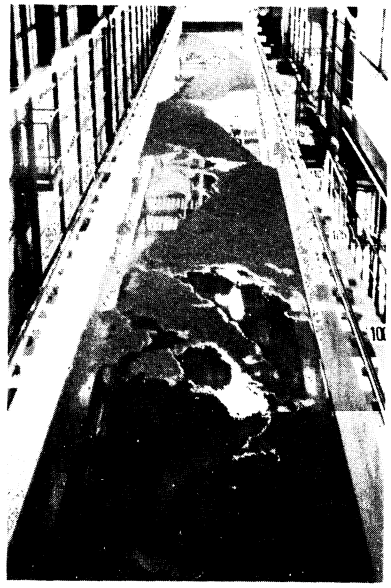

Fig. 3-18 Downstream view of short diagonal bars at end of Run 20 ($S = 1/200$, $Q = 1.0\ m^3/sec$) The water surface is more turbulent than in the preceding run.

Fig. 3-19 Upstream view of low relief dunes, or antidunes, at end of Run 28 ($S = 1/200$, $Q = 1.5\ m^3/sec$)

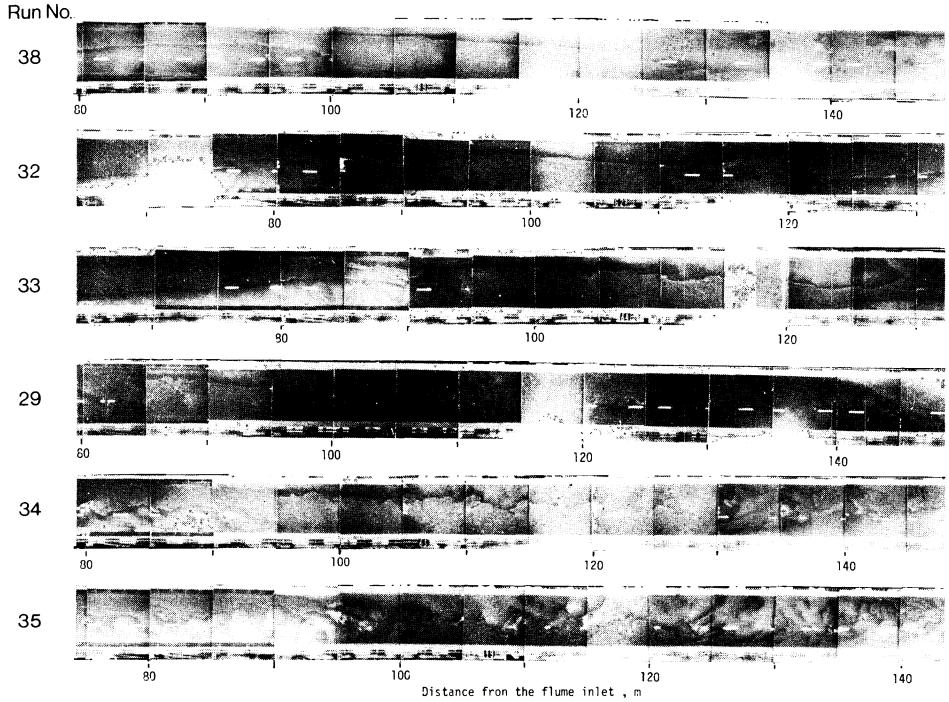

Fig. 3-20-1 Changes in the shape of bed configurations with increasing discharge at slope 1/400 (Case 3)

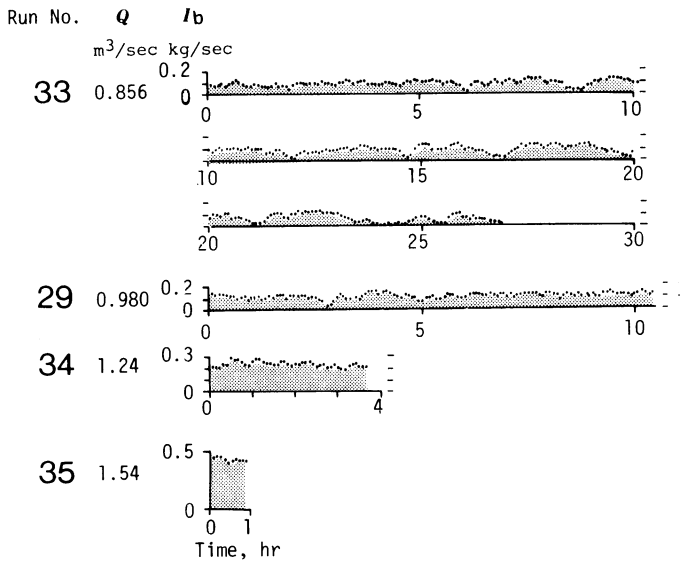

Fig. 3-21 Changes in bed material discharge at slope 1/400 (Case 3)

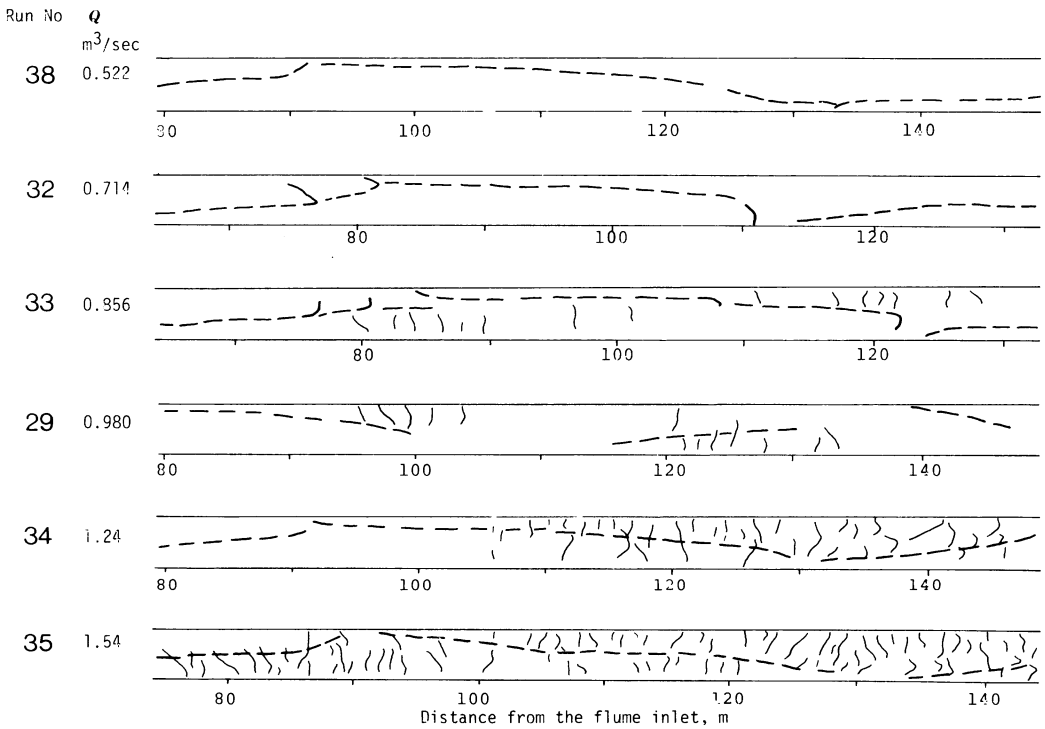

Fig. 3-20-2 Changes in the shape of bed configurations with increasing discharge at slope 1/400 (Case 3)

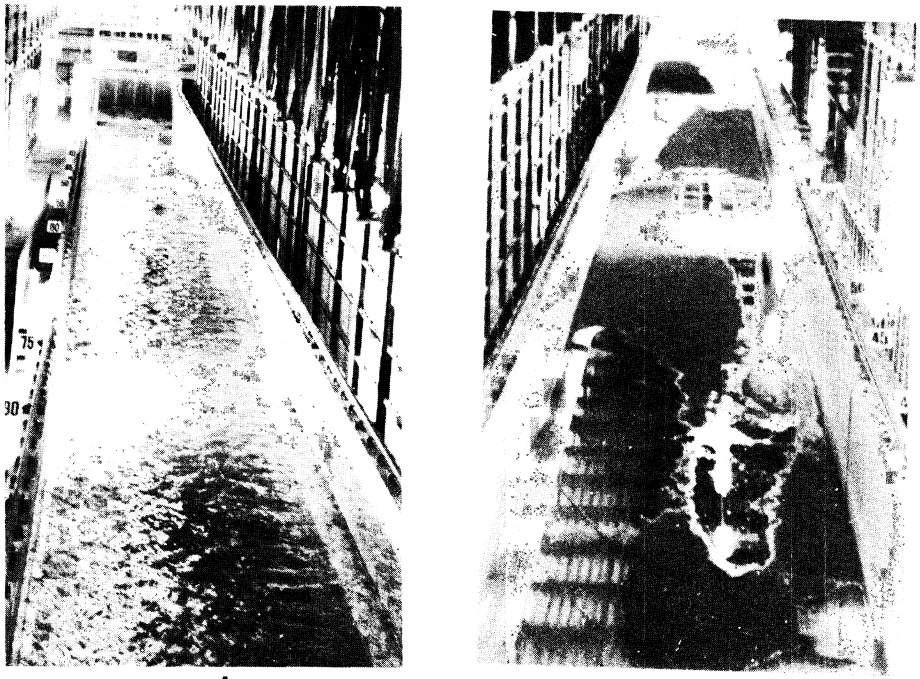

Fig. 3-22 Flow and bed conditions for Run 32 (S = 1/400, Q = 0.7 m^3/sec)
(A) Upstream view of bumpy water surface
(B) Downstream view of alternating bars at end of run

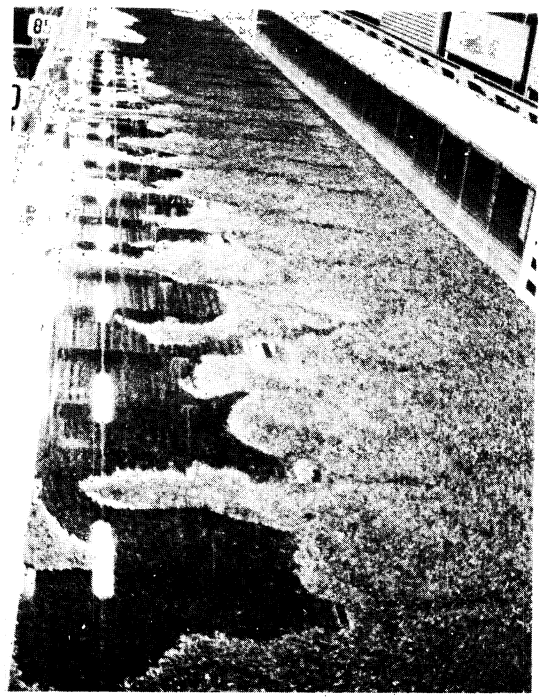

Fig. 3-23 Low-relief dunes formed during Run 29 (S = 1/400, Q 1 m^3/sec)

become unclear and instead, low-relief dunes developed on the bed (Fig. 3-23). The length and height of the dunes were observed to be 1.5 to 2 meters long and only 2 to 4 centimeters high. Although the discharge was large, the water surface was relatively smooth, but low bumpy standing waves were seen (Fig. 3-24).

3-4 Development of bars on flat beds of fine gravel (Case 4)

Each run was started with the bed fixed at a slope of 1/100. The range of flow depth was between 5 cm to 10 cm. Experimental conditions are shown in Table 3-1.

When the discharge was less than 0.18 m^3/sec, that is, the depth was less than 5 cm, no sediment was transported on the carefully planed bed of fine gravel.

When the discharge was more than 0.18 m^3/sec, longitudinal striations (Fig. 3-25) and small antidunes occurred on what was essentially a flat bed.

Further increase in discharge caused the development of rhomboid bars and antidunes (Figs. 3-26A and 3-27A). As flow continued, rhomboid bars immediately merged into larger rhomboid bars (Figs. 3-26B and 3-27B). Rhomboid bars have high wave-length/height ratios, and are straight-crested. However, under these flow conditions, alternating bars are a more stable bed configuration, and with time, rhomboid bars gradually changed into alternating bars with curved crests and long wavelength (Figs. 3-26C, 3-28 and 3-29). Flow over alternating bars distinctly meandered inspite of being in the straight flume (Fig. 3-30). The wavelength of alternating bars increased with longer flow duration. Eventually, parts of the bars emerged onto the water surface and no more bar movement was observed (Fig. 3-31).

Table 3-1 Experimental conditions for Case 4

Run No.	S $\times 10^{-2}$	Q l/sec	T_W °C	V cm/sec	D cm	T
5	1.00	184	14.0	82	5.6	17 min
6	1.00	235	14.0	93	6.3	11 min
4	1.00	314	12.0	87	9.0	16 min
2	1.02	386	11.5	90	10.7	10 min
7	1.04	518	14.0	109	11.9	4 min
81	1.02	352	15.0	100	8.8	17 hr
80	1.04	402	20.5	97	10.4	30 hr

T: total duration of run

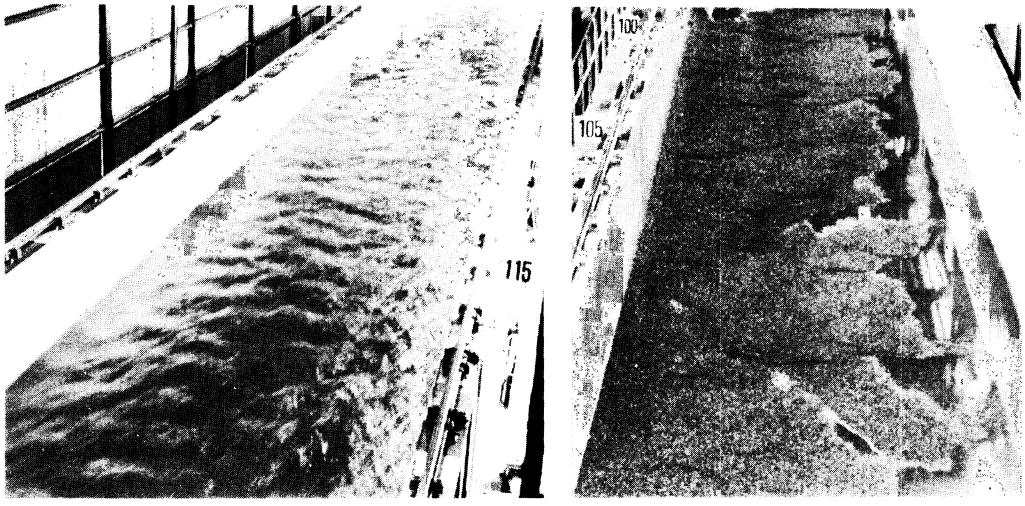

Fig. 3-24 Flow and bed conditions for Run 34 (S = 1/400, Q = 1.24 m^3/sec)
(A) Downstream view of water surface condition
(B) Upstream view of low relief dunes

Fig. 3-25 Plan view of longitudinal striations for Run 81 (S = 1/100, Q = 0.35 m^3/sec)
The flow is from left to right.

A

B

C

Fig. 3-26 Upstream views of bed configurations for Run 80 (S = 1/100, Q = 0.4 m^3/sec)
(A) 7 minutes after start of run
(B) 32 minutes after start of run
(C) 73 minutes after start of run

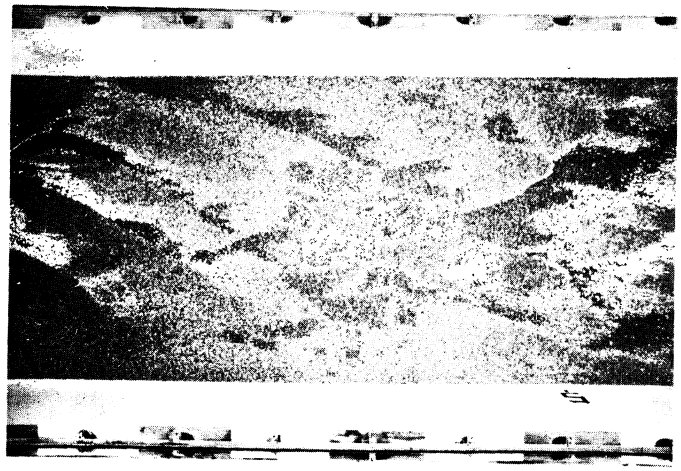

A

B

Fig. 3-27 Plan views of rhomboid bars for Run 80 (S = 1/100, Q = 0.4 m^3/sec)
(A) 7 minutes after start of run
(B) 39 minutes after start of run
The flow is from left to right

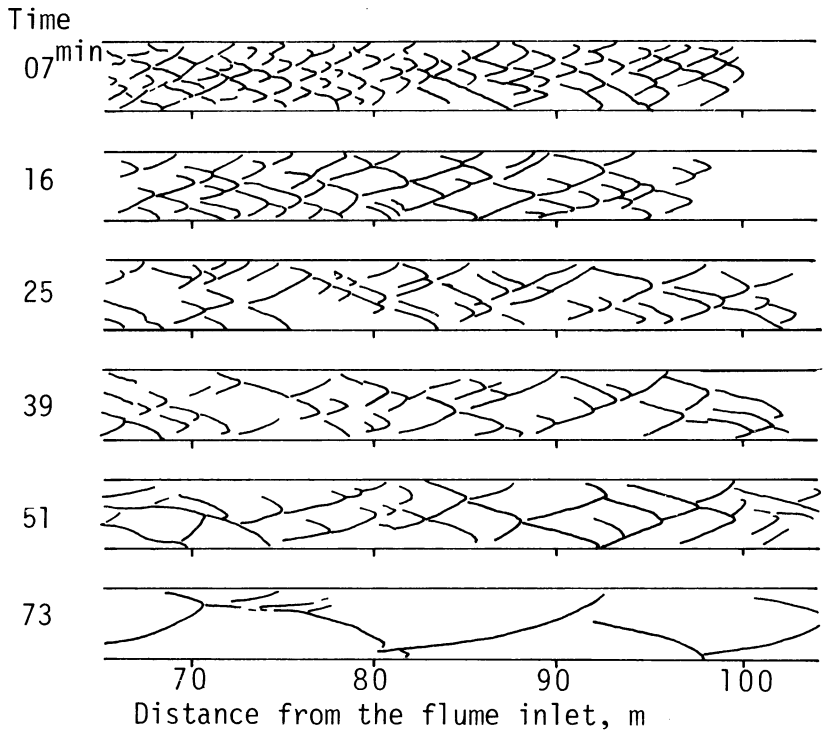

Fig. 3-28 Time change in bar-bed configurations for Run 80 (S = 1/100, Q = 0.4 m^3/sec) The flow is from left to right.

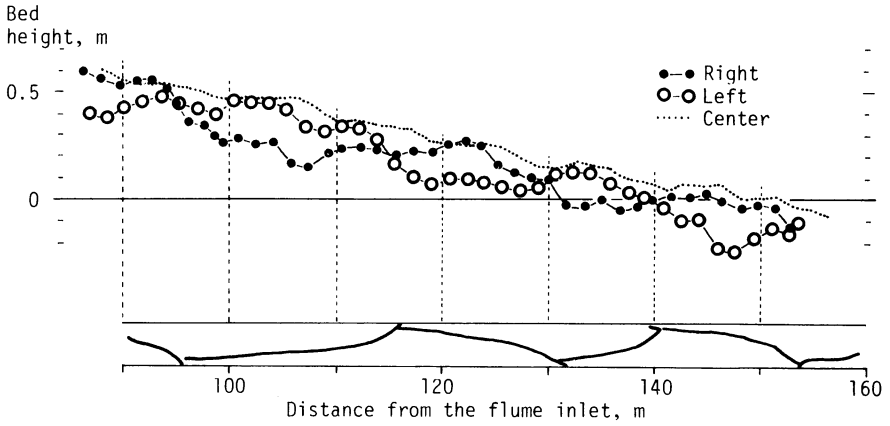

Fig. 3-29 Bed surface profiles of alternating bars for Run 80 (S = 1/100, Q = 0.4 m^3/sec). A characteristic of run 80, is that the bed height along the center of the flume is higher than the left and right sides. This is quite different from the profile of typical alternating bars.

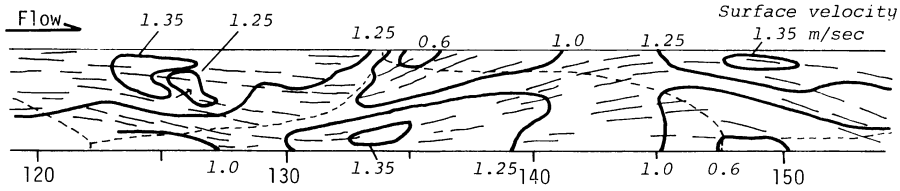

Fig. 3-30 Distribution of surface velocity and flow direction over alternating bars for Run 80, by means of multiple exposure photographic technique (S = 1/100, Q = 0.4 m³/sec)

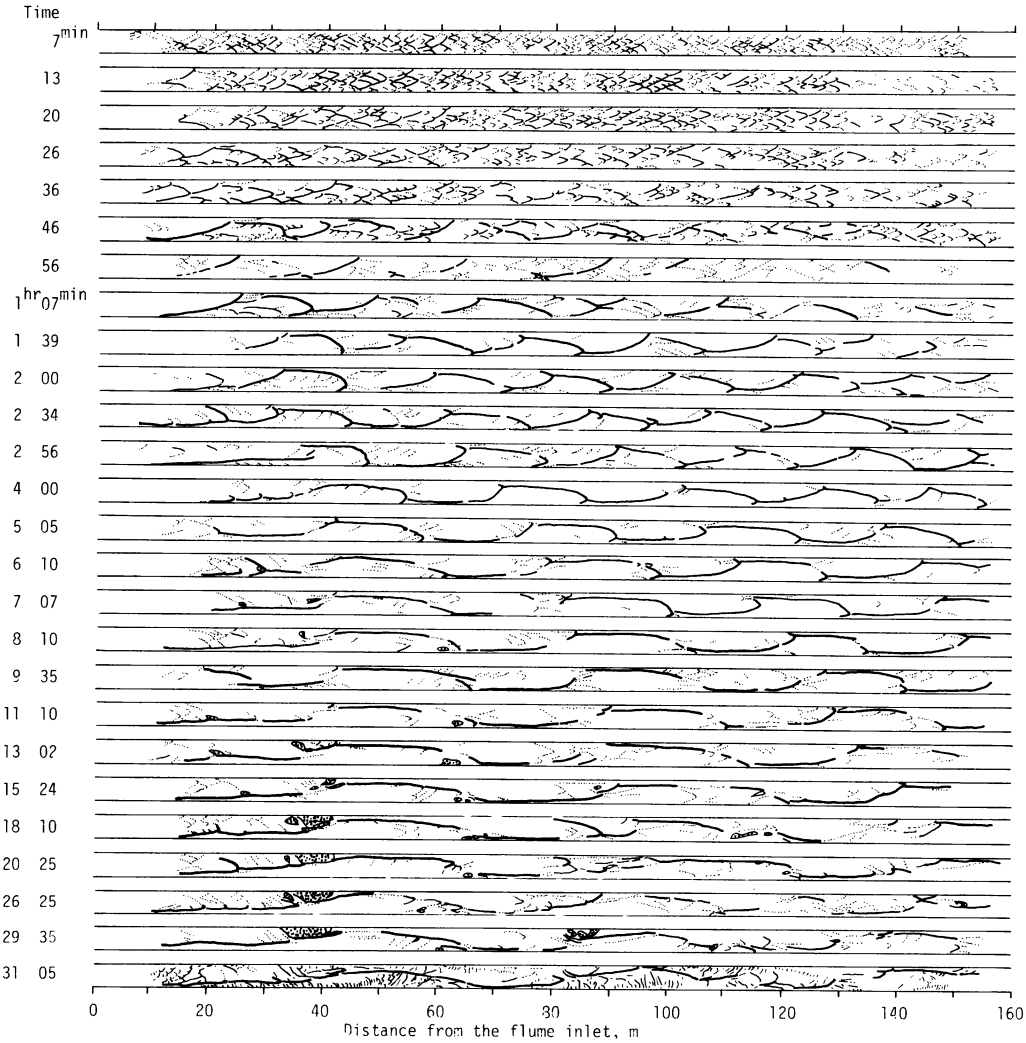

Fig. 3-31 Development of alternating bars for Run 81 (S = 1/100, Q = 0.35 m³/sec)
Observation of bed configuration at the last (T=31 hr.) was made at the end of the run, after the water had been drained out.

CHAPTER 4

BEDLOAD TRANSPORT

4-1 Bedload transport of fine gravel in the 4-meter-wide flume

In 1970, Williams succeeded in isolating the effect of wall drag in a flume in his sediment transport experiments. On the basis of his results, Bagnold (1973) pointed out that the bedload transport rate has a dependence on the flow depth, that is, the increase of transport with decrease of flow depth at the same stream power is not due to the wall drag as it had often been supposed, but is due to an inherent property of the bedload transport mechanism.

If Bagnold's assertion is true, transport rates measured in small laboratory flumes can not be applied to flows of greater depth, without considerable modifications. Since then, the effect of flow depth or slope on sediment transport has attracted special interest (Vanoni, 1975).

In order to evaluate accurately the effect of flow depth or slope on the bedload transport rate, it is necessary to eliminate not only the effect of wall-drag, but also the effect of bed forms. It is a matter of regret that the bed forms from Williams' data ranged from dunes to antidunes.

As shown in Figs. 3-1-14, 3-13-25, and 3-20-21, bed configurations at the same stream power are dependent on slope. Thus, the steeper the slope, the more the three-dimensionality of the flow, and the more the number of bars. However, most of the bed configurations within the bedload transport experiments in fine gravel were bars, low relief dunes and antidunes. Therefore, under the nearly analogous low relief bed configurations and low depth/grain-size ratio conditions, we were able to obtain a set of data on the bedload transport in which the effects of the flume side walls could be ignored.

Many of the existing sediment formulae are based on the local balance of the forces acting on a sediment particle in water. Though this type of approach is microscopic, it gives us reasonable results for uniform, small laboratory flumes. A more practical approach is necessary for the sediment transport study of natural rivers, as natural river channels are by no means uniform.

Even in the 4-meter-wide straight laboratory flume, the bedload transport rate changed transversely in the cross-section of the channel, due to the formation of alternating bars (Figs. 4-1 and 4-2). Fig. 4-3 shows the bedload sampler used.

Therefore, to discuss these three-dimensional transport phenomena, it is satisfactory to apply the idea of Bagnold (1977). In other words, when the flume is regarded as a transporting machine, the bedload transport rate in the flume has much dependence on the stream power, the rate of energy input into the flume system.

4-2 The relationship between the bedload transport rate and the stream power

Measured transport rates (I_b) for Case 1, Case 2, and Case 3 are plotted against the stream power (Ω) in Fig. 4-4. As shown by these figures, at any given value of stream power, the transport rate I_b apparently decreases with a decrease in slope, especially when the stream power is small.

Moreover, a certain power called threshold stream power, Ω_0, exists in each case, above which the bed material begins to move. The steeper the slope is, the lower the amount of threshold

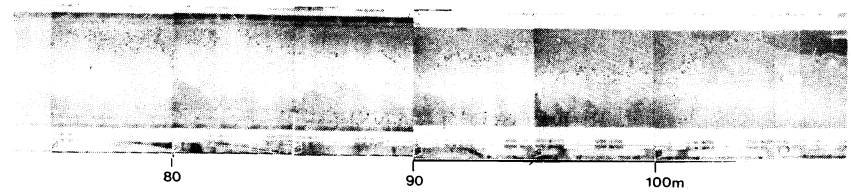

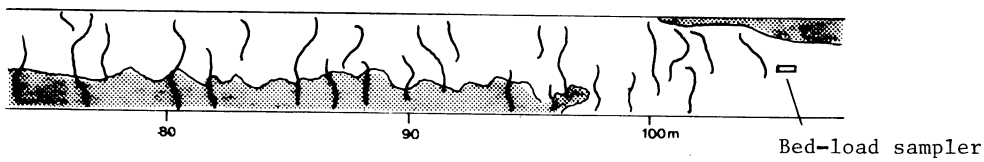

Fig. 4-1 Plan view showing position of measured section for bedload transport rate (S = 1/400, Q = 1 m³/sec)

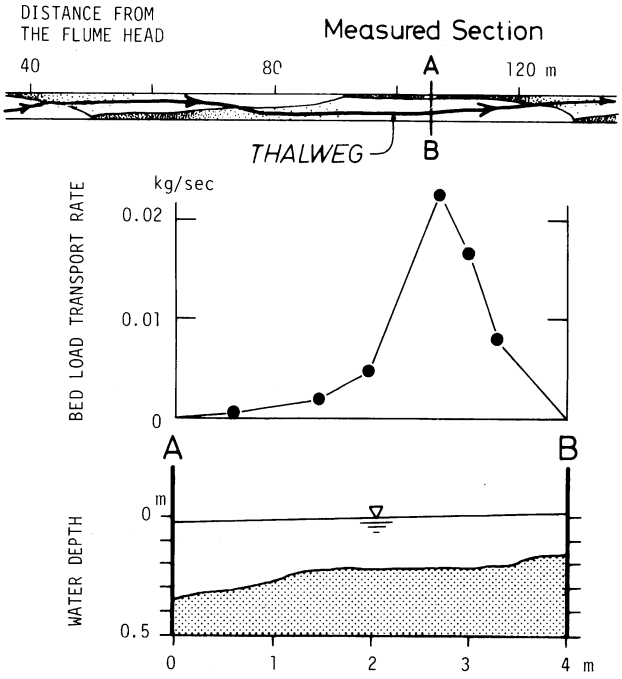

Fig. 4-2 Transverse distribution of bedload transport rate over alternating bars (S = 1/400, Q = 1 m³/sec)

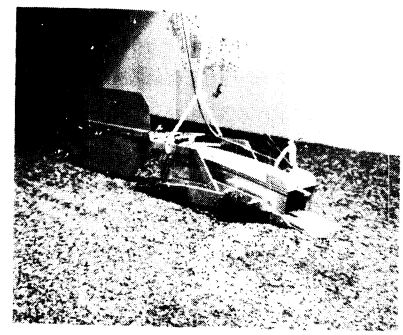

Fig. 4-3 "Doken"-type bedload sampler used The total length is 1.6 meters.

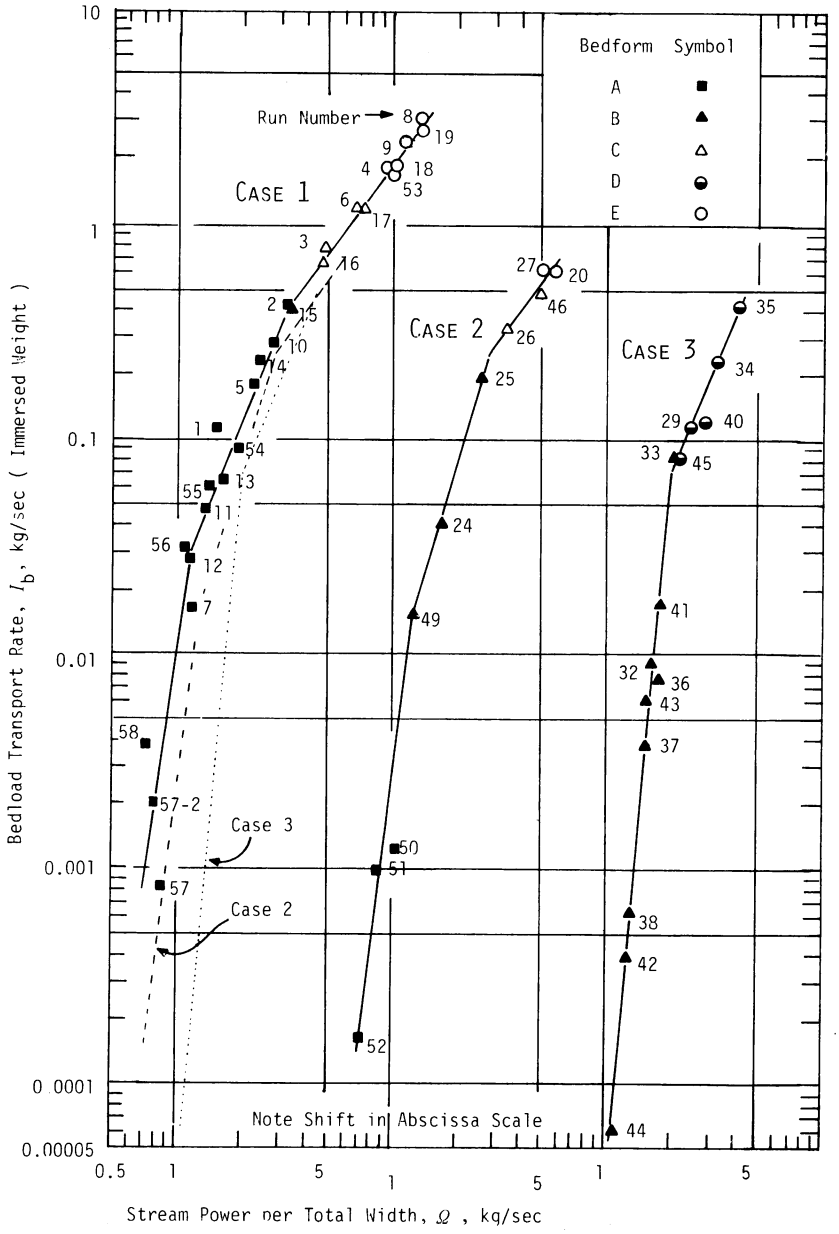

Fig. 4-4 Experimental data for fine gravel plotted as bedload rate I_b versus stream power per unit length of the channel Ω, showing increase in I_b due to increase in slope in spite of the constant Ω

Bed states:

A, multiple row bars; B, alternating bars; C, alternating bars with standing waves; D, low-relief dunes; E, antidunes

power there is. The threshold stream power corresponding to the planed bed condition is about 2 kg/sec, which is confirmed in the runs in Case 4, but is only 0.3 kg/sec when the slope is 1/100, 0.5 kg/sec when the slope is 1/200, and 1.0 kg/sec when the slope is 1/400. The reason for the differences between the values of Ω_0 in Cases 1, 2, and 3 and the value of Ω_0 in planed bed conditions, is owing to the converging of the flow caused by the presence of bed undulations. The point which I would especially like to emphasize here, is the fact that the threshold power for undulated beds is a variable which depends upon the slope.

4-3 The relationship between the bedload transport rate and the available power

The threshold power Ω_0 is considered to be dissipated to maintain the flow against the resistance. Hence, it is reasonable to consider that an excess power, that is, the stream power Ω minus the threshold power Ω_0, is the available power for the bedload transport (Bagnold, 1966, 1977). Ω_0 is a value of approximation to the smallest measured Ω at which traces of bedload transport is detectable.

After the data were replotted in the I_b to $\Omega - \Omega_0$ relation, it was found that the plots arranged themselves approximately in a line, despite the different values of the slopes.

These results showed conclusively that the increase of the transport rate with an increase of slope, at the same stream power, is partly due to a decrease in the threshold stream power, hence, increasing the amount of available power. Making clear, quantitatively, how the amount of the threshold power on an undulating bed varies with slope and depth, is an important factor for the computation of the bedload transport rate (especially when the stream power is small), and is a future topic for study.

Furthermore, for the runs in which the water temperature was between 10°C and 25°C (Table 2-1, Case 1), the effects of the water temperature on the bedload transport rate for fine gravel were investigated, but no difference was found.

4-4 The proportionality of the bedload transport rate to the available power

The proportionality between the bedload transport rate and the 3/2 power of excess or available stream power was obtained empirically by Bagnold (1977) at constant flow depth/grain-size ratio. However, the exponent at high transport stage in Fig. 4-5 is 4/3, which is smaller than 3/2.

As pointed out by Ikeda and Inokuchi (1979), the exponent in the relationship between I_b and $\Omega - \Omega_0$ at high transport stage is changed depending on the combination of the discharge and slope. In other words, if the stream power is increased by augmenting the discharge and the slope at a constant water depth, the exponent becomes 3/2, as shown by the W in Fig. 4-6. However, at a constant slope, increasing the discharge and making the stream power larger, makes the exponent closer to 1, which is smaller than 3/2, as shown by the I in Fig. 4-6. On the other hand, at constant discharge, increasing the slope and making the stream power larger, makes the exponent closer to 2, which is larger than 3/2, as shown by the K in Fig. 4-6. This means that the bedload transport rate is proportional to the discharge and to the square of the slope.

In an alluvial river channel, the stream power at a station increases chiefly due to an increase of discharge, and not due to change in slope. Consequently, it is thought that the exponent becomes smaller than 3/2 and closer to 1, at high transport stage.

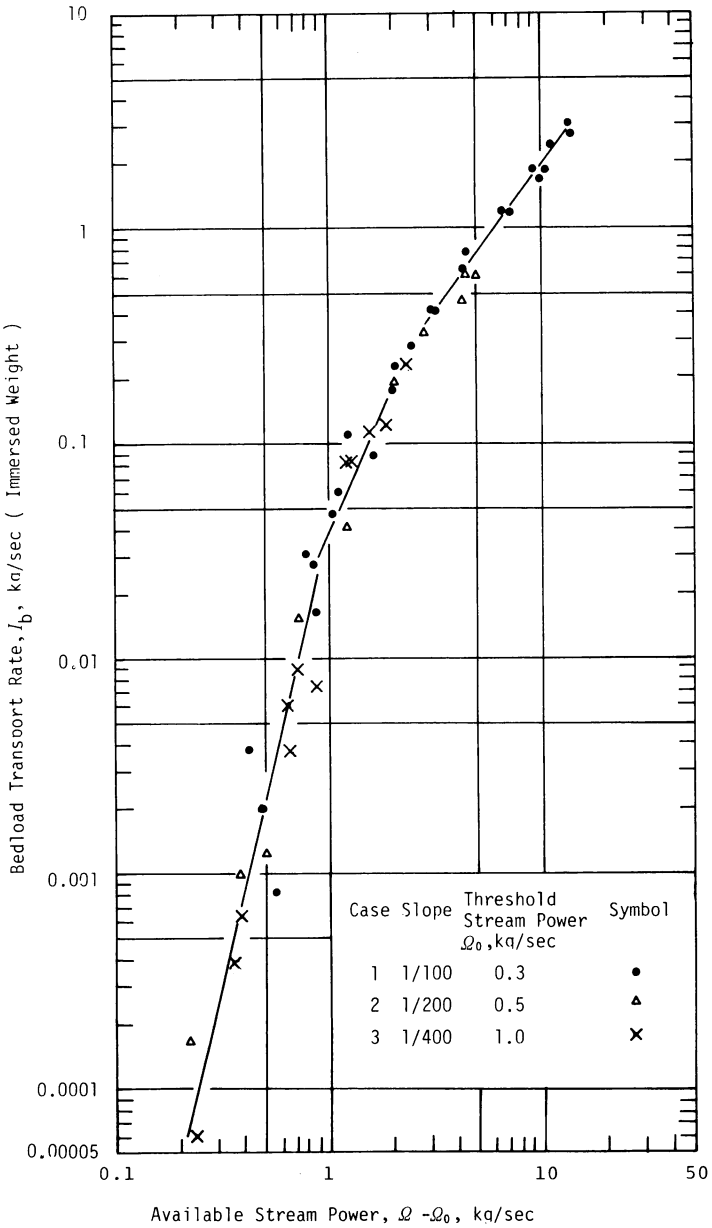

Fig. 4-5 Data of Fig. 4-4 replotted with available stream power Ω, substituted for stream power, $\Omega - \Omega_0$. Threshold stream power was taken as 0.3 kg/sec for S = 1/100, 0.5 kg/sec for S = 1/200, and 1.0 kg/sec for S = 1/400.

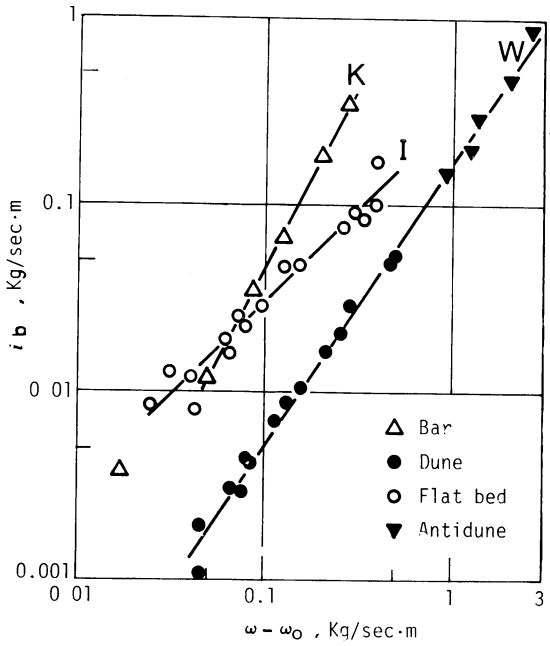

Fig. 4-6 Relationship between bedload transport rate per unit width, i_b, to available stream power per unit bed area, $\omega - \omega_0$.
W: Williams (1970), d_m = 1.24 mm, D is held constant
K: Kinoshita (1962), d_m = 1.10 mm, $q = Q/W$ is held constant
I: Ikeda (1978), d_{s0} = 1.10 mm, S is held constant

4-5 The effect of the width/depth ratio of flow on the bedload transport rate

When a fixed amount of water flows over a bed with a constant slope, how would the amount of bedload transported by the water flow vary with the width of the flow? From the fact that rivers with a high bedload transport rate generally have a high width/depth ratio, it was thought that the wider the water flow, the higher the bedload transport rate (Griffith, 1927; Lane, 1937).

Bagnold (1977) also thought that the larger the width/depth ratio, the higher the bedload transport rate. This was because he concluded that, at any given value of available power and grain size, the bedload transport rate decreases as an inverse function of the flow depth. Then, Bagnold considered that, at any given discharge and slope, the wider an alluvial river is, the shallower the depth of the flow becomes, and consequently, the greater the rate at which it can transport a bedload of a given mean grain size.

Ikeda (1978) investigated the effect of the flume width on the bedload transport rate. In his experiment, the flume width was varied in 7 stages, between 1 cm and 40 cm, while maintaining a constant slope of 1/50 (Table 4-1). The experimental results are shown in Figs. 4-7 and 4-8. Fig. 4-7 shows the effect of the flume width on the bedload transport rate. Fig. 4-8 shows the effect of the flume width on the bedload transport rate, at any given stream power.

In a flow where the width/depth ratio is extremely small (Zone I in Fig. 4-8 whose width/depth ratio is less than 1.5), the stream power is dissipated due to the wall drag. Hence, the wider the width, the less the wall drag, and as the available stream power used for bedload transport increases, so does the bedload transport rate. Thus, the bedload transport efficiency is increased.

In Zone II in Fig. 4-8 which has a high width/depth ratio, the bedload transport rate decreases

Table 4-1 Experimental results on effect of width/depth ratio of flow on bedload transport rate ($S = 1/50, d_{50} = 1.1$ mm)

Run No.	Q l/sec	D cm	I_b g/sec	Bed state
Flume width: 1cm				
1-1	0.105	2.55	0.098	P
2	0.154	3.70	0.161	P
3	0.264	5.34	0.264	P
Flume width: 2cm				
2-1	0.018	0.45	0.000	P
2	0.030	0.65	0.000	P
3	0.058	1.05	0.157	P
4	0.126	1.97	0.360	P
5	0.195	2.50	0.456	P
6	0.315	3.46	0.507	P
7	0.422	4.18	0.574	P
8	0.645	5.92	0.685	A
9	0.867	7.07	0.753	A
10	1.06	7.66	0.803	A
11	1.34	11.2	0.828	A
12	1.70	12.0	0.934	A
Flume width: 3cm				
3-1	0.100	1.18	0.182	P
2	0.147	1.45	0.592	P
3	0.224	1.93	1.09	P
4	0.313	2.25	1.10	A
5	0.419	2.51	1.54	A
6	0.570	3.36	1.41	A
7	0.593	3.50	1.38	A
8	0.692	3.73	1.51	A
9	0.954	4.88	2.38	A
10	1.21	5.21	2.80	A
11	1.53	6.60	3.29	A
12	1.77	7.44	3.56	A
13	2.12	8.88	4.13	A

Run No.	Q l/sec	D cm	I_b g/sec	Bed state
Flume width: 5cm				
5-1	0.037	0.583	0.000	P
2	0.071	0.683	0.027	P
3	0.081	0.783	0.105	P
4	0.123	0.900	0.222	P
5	0.164	1.15	0.604	P
6	0.203	1.35	0.809	P
7	0.237	1.45	1.08	P
8	0.270	1.50	0.828	P
9	0.534	2.36	2.26	P
10	0.929	3.20	2.49	A
11	0.60	4.13	6.16	A
12	2.40	5.41	13.3	A
Flume width: 10cm				
10-1	0.062	0.550	0.000	P
2	0.072	0.650	0.000	P
3	0.117	0.750	0.026	B
4	0.148	0.830	0.182	B
5	0.191	–	0.386	B
6	0.230	1.05	0.853	P
7	0.264	1.30	1.30	P
8	0.313	1.00	1.24	P
9	0.324	1.10	0.816	P
10	0.417	1.10	1.96	P
11	0.437	1.40	1.64	P
12	0.472	1.43	2.55	P
13	0.505	1.45	2.28	P
14	0.602	1.50	2.95	P
15	0.755	1.72	4.73	P
16	0.886	2.11	4.81	P
17	1.08	2.16	3.70	P
18	1.21	2.20	4.60	P
19	1.41	2.48	7.91	P
20	1.64	2.76	9.40	P
21	1.81	2.88	8.53	P
22	2.06	3.10	10.2	P
23	2.13	3.10	17.7	P

Run No.	Q l/sec	D cm	I_b g/sec	Bed state
Flume width: 20cm				
20-1	0.180	–	0.000	P
2	0.240	(0.87)	0.413	B
3	0.302	(1.00)	0.215	B
4	0.345	(1.33)	0.196	B
5	0.417	(1.48)	0.884	B
6	0.426	–	0.660	B
7	0.480	(1.40)	1.58	B
8	0.558	(1.38)	2.37	B
9	0.733	(1.54)	2.48	B
10	0.820	–	2.68	B
11	1.10	(1.55)	5.61	B
12	1.33	(1.61)	5.57	B
13	1.57	(1.83)	6.85	B
14	1.88	(1.87)	10.1	B
15	2.05	(1.88)	10.2	B
16	2.24	(2.06)	11.2	B
Flume width: 40cm				
40-1	0.341	–	0.349	B
2	0.527	–	0.922	B
3	0.529	–	1.49	B
4	0.624	–	1.57	B
5	0.732	–	2.51	B
6	0.790	–	1.59	B
7	0.979	–	2.54	B
8	1.28	–	5.16	B
9	1.49	–	8.72	B
10	1.65	–	5.12	B
11	1.76	–	4.81	B
12	1.88	–	12.0	B
13	1.89	–	6.08	B
14	2.02	(0.94)	8.97	B
15	2.10	(1.52)	5.11	B
16	2.13	–	14.9	B
17	2.34	1.26	9.28	B

Bed state:
P, plane bed; B, bars; A, antidunes
– : not measured

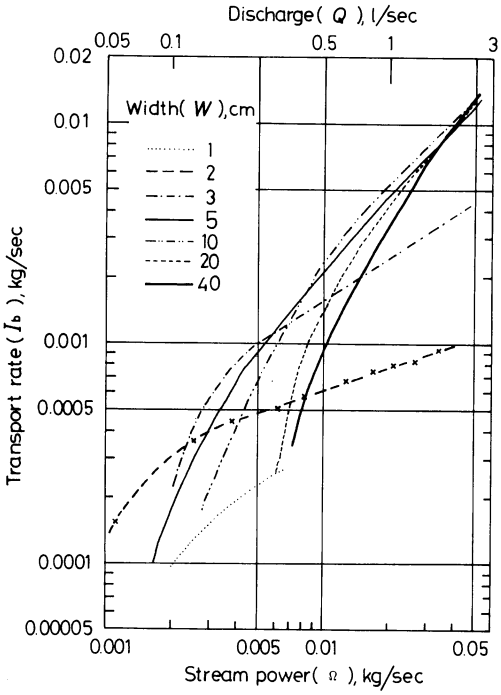

Fig. 4-7 Effect of flume width on relationship between bedload transport rate I_b, and stream power per total width Ω (S = 1/50, d_{50} = 1.1 mm)

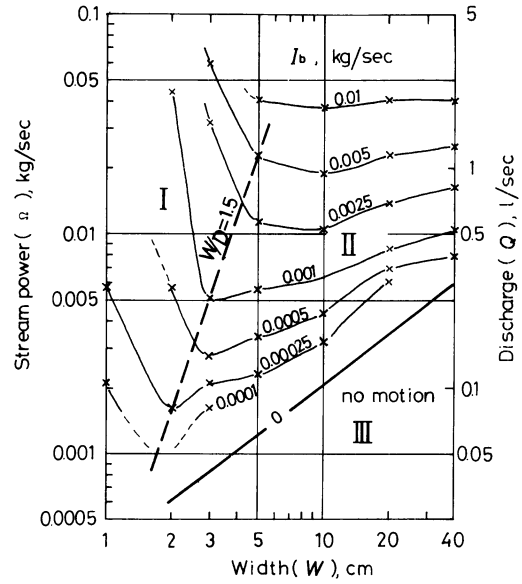

Fig. 4-8 Effect of flume width on the bedload transport rate at any given stream power

as the flume width increases. This is because the critical stream power for the bed material movement increase nearly proportionally to the width of the flow, and because the available power for the bedload transport decreases. A normal natural river must correspond to that of Zone II in Fig. 4-8. Therefore, by increasing the flow width with a given stream power, the bedload transport rate should decrease.

It can be stated that, at the same stream power, the shallower the depth is, the higher the bedload transport rate becomes, but this is true only when the width is kept constant, and the slope is increased, and the water depth is decreased.

CHAPTER 5

RHOMBOID BARS

5-1 Rhomboid bars formed in the 4-meter-wide flume

As shown in Fig. 5-1, when water was made to flow for a short time over a planed bed, longitudinal elements called longitudinal striations or sand ribbons (Allen, 1968), transverse elements called antidunes, and oblique and fish-scale patterns called rhomboid bars, were formed in the 4-meter-wide flume. Among these, longitudinal striations and antidunes were generated at lower discharges and sometimes presented a grid-iron pattern (Runs 5 and 6). After rhomboid bars developed, antidunes diminished and longitudinal striations also became obscured (Runs 4, 2 and 7).

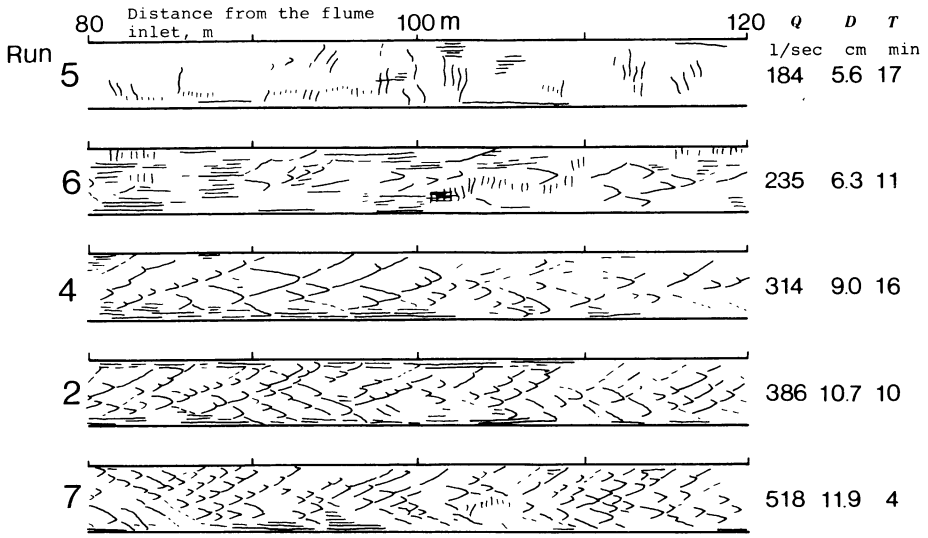

Fig. 5-1 Plan view of rhomboid bars in the 4-meter-wide flume (Case 4) (S = 1/100, d = 6.4 mm)
The flow is from left to right.

From these facts, it can be assumed that oblique crests of rhomboid bars may be formed by the combination of longitudinal striations and antidunes. If this assumption is correct, as a most simple explanation, one can assume the longitudinal striations and antidunes to be waves which intersect perpendicularly, and that the oblique crests are waves in the direction of the diagonal, caused by this combination. From this, the following equation can be expected:

$$\beta = \tan^{-1}\frac{L_l}{L_t} \quad \cdots\cdots\cdots\cdots\cdots\cdots\cdots\cdots\cdots\cdots\cdots\cdots\cdots\cdots \quad (5\text{-}1)$$

where, β : the angle between rhomboid bar crests and flume side walls,
L_l : the spacing of the longitudinal striations, and
L_t : the wavelength of the antidunes.

5-2 Spacing of longitudinal striations and wavelength of antidunes

Experiments to determine whether the assumption made for equation 5-1 was suitable or not, were performed in a tilting small laboratory flume 9 m long, 0.2 m wide, and 0.06 m deep. 25 runs were made with uniform, coarse sand. The median grain size was 0.81 mm. In each run, a sand bed of 3 cm thickness was placed in the flume and was carefully leveled. The water was made to flow for a few minutes. Quantities measured and derived are given in Table 5-1.

Table 5-1 Summary of experimental data on formation of rhomboid bars in the 0.2-meter-wide flume (d_{50} = 0.81 mm)

Run No.	S	Q cc/sec	T_W °C	V_S cm/sec	D cm	V cm/sec	F	L_l cm	L_t cm	β °	Stable bed state
201	0.0482	628	14.0	32.3	1.10	28.5	0.869	–	–	20.0	P
202	〃	800	14.0	36.3	1.34	29.9	0.824	2.5	6.0	23.9	P
203	〃	975	14.5	38.7	1.50	32.5	0.848	–	–	25.6	P
204	〃	1371	14.5	41.5	1.91	35.9	0.830	4.0	8.0	26.7	P
141	0.0731	700	16.7	38.0	1.08	32.4	0.996	2.2	–	19.8	P
142	〃	1245	16.7	46.5	1.60	38.9	0.983	3.3	8.3	22.0	P
101	0.0103	493	–	36.6	0.80	30.8	1.10	1.7	5.7	13.4	P
102	〃	830	16.0	45.1	1.20	34.6	1.01	–	6.2	22.9	P
103	〃	1238	16.0	49.6	1.45	42.7	1.13	–	8.7	22.0	A
71	0.0131	302	13.0	34.5	0.53	28.5	1.25	–	4.1	13.8	P
72	〃	338	13.0	35.9	0.60	27.3	1.13	1.2	4.3	16.4	–
73	〃	356	10.0	35.3	0.68	26.2	1.01	1.3	4.3	14.8	B
74	〃	377	10.0	–	0.68	27.7	1.07	1.3	4.6	16.8	B
75	〃	582	–	42.3	0.90	32.3	1.09	1.8	6.5	18.3	P
76	〃	712	–	44.1	1.00	35.6	1.14	–	–	20.7	P
51	0.0197	192	12.0	30.3	0.35	27.4	1.48	–	3.8	7.0	D
52	〃	283	16.0	35.3	0.45	31.4	1.50	–	3.8	12.3	D
53	〃	498	15.0	43.3	0.70	35.6	1.36	–	6.0	12.5	D
54	〃	727	15.0	43.5	0.90	40.4	1.36	–	6.9	15.3	D
55	〃	1223	15.0	62.5	1.24	49.3	1.41	–	8.3	14.3	A
31	0.0285	102	–	35.3	0.19	26.8	1.97	–	3.0	5.5	D
32	0.0288	181	14.5	–	0.34	25.8	1.40	–	3.6	9.0	D
33	〃	238	–	38.5	0.37	32.2	1.69	–	3.7	9.4	D
34	0.0285	251	–	43.2	0.45	27.9	1.33	–	3.5	14.5	D
35	〃	455	12.0	44.8	0.60	37.9	1.56	–	3.9	16.6	D

– : not measured

Stable bed state:

A, antidunes; B, alternating bars; D, double row bars; P, plane bed with diagonal bars superposed

Longitudinal ridges and furrows resulted from patterns of eddying in the flow. Spiral eddies had axes parallel to the current. Adjacent eddies had opposite rotations so the flow at the bed had zones of alternating upward and downward directed components. The line along which the descending vortices impinge on the bed will be the site for the occurrence high stress and longitudinal scours (Figs. 5-2 and 5-3).

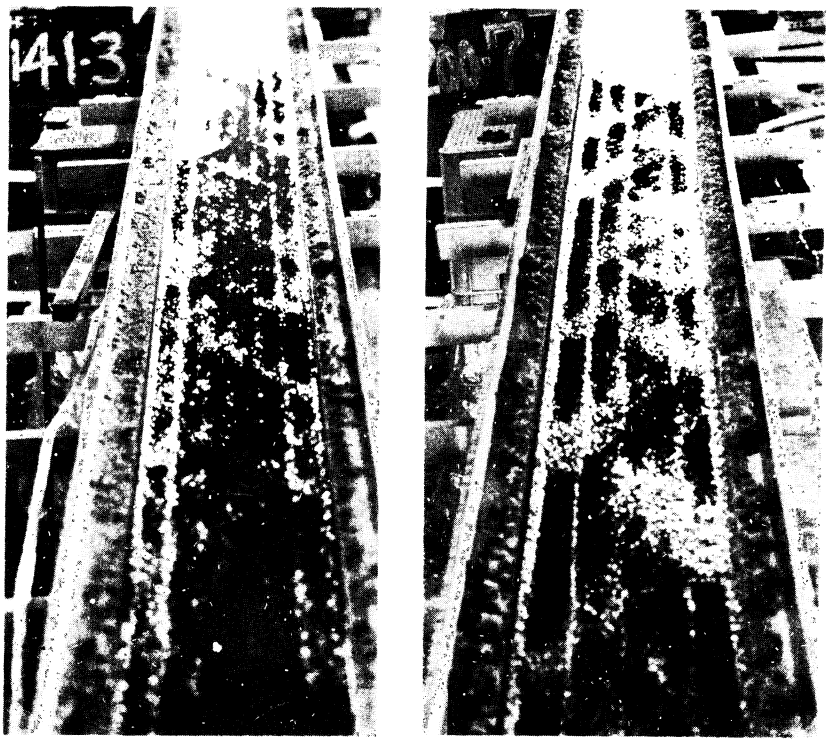

Fig. 5-2 Upstream views of longitudinal striations
(A) Run 142, S = 1/140, D = 1.6 cm
(B) Run 204, S = 1/200, D = 1.9 cm

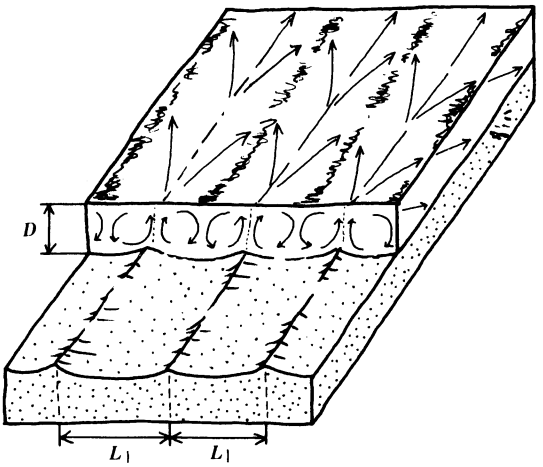

Fig. 5-3 Pattern of flow associated with development of longitudinal striations

Vertical sections of spiral eddies are nearly circular shapes. Therefore, it is a well known fact that the spacing of longitudinal ridges are 2 times the flow depth (Kinoshita, 1962). As shown in Fig. 5-4, the spacing of longitudinal striations L_l is dependent only on the water depth, and not on the slope or the size of the bed material.

$$L_l = 2D \quad \cdots\cdots\cdots\cdots\cdots\cdots\cdots\cdots\cdots\cdots\cdots\cdots\cdots\cdots \quad (5\text{-}2)$$

where, D : depth of water.

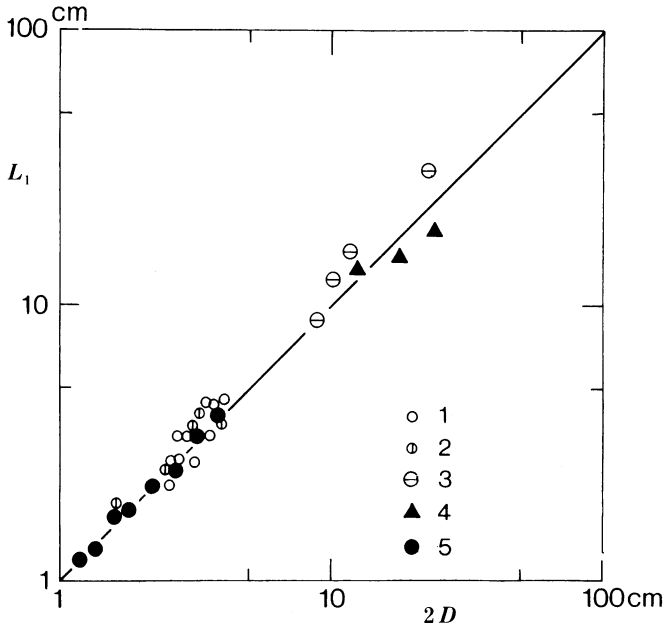

Fig. 5-4 Relationship between flow depth and spacing of longitudinal striations
1: Kinoshita (1962), 2: Wolman and Brush (1961), 3: Vincent (1967),
4: the 4-meter-wide flume, 5: the 0.2-meter-wide flume

On the other hand, for the wavelength of antidunes (Fig. 5-5), the below equation was given by Kennedy (1961, 1963).

$$L_t = \frac{2\pi}{g} \cdot V^2 \quad \cdots\cdots\cdots\cdots\cdots\cdots\cdots\cdots\cdots\cdots\cdots\cdots\cdots\cdots \quad (5\text{-}3)$$

where, L_t : wavelength of antidunes,
V : mean velocity of flow,
g : gravitational constant.

This equation, which is identical with the celerity-wavelength relation for gravity waves in a deep fluid, has been found to give fairly reliable results for flows in laboratory flumes (Kennedy, 1961) and in natural alluvial channels (Nordin, 1964). As shown in Fig. 5-6, the experimental values agree with the calculated values for flows in laboratory flumes, except when the flow was very steep.

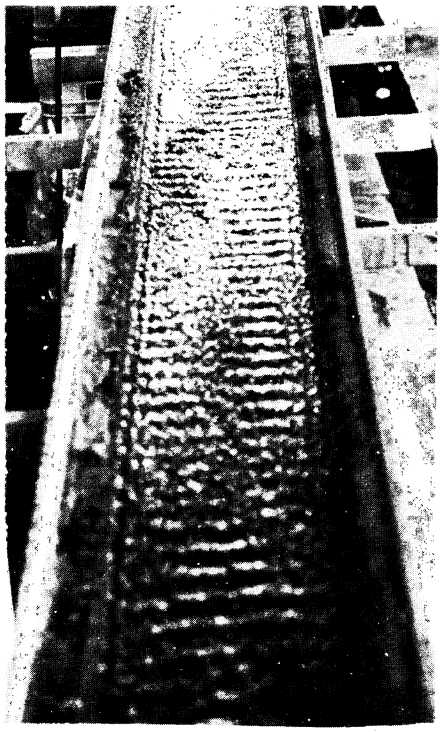

Fig. 5-5 Upstream view of small antidune waves for Run 101 (S = 1/100, D = 0.8 cm)

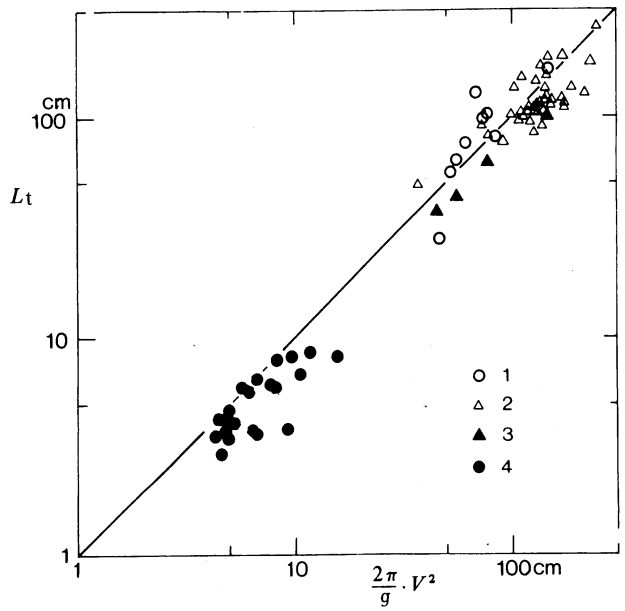

Fig. 5-6 Comparison of the experimental results of antidune wavelengths with calculated values
1: Tanaka (1970), 2: Guy, et al. (1966), 3: the 4-meter-wide flume experiments,
4: the 0.2 meter-wide flume experiments

5-3 Rhomboid bars formed by the interaction of longitudinal and transverse elements

As shown in Fig. 5-7, even in a small flume, the combination of longitudinal striations and antidunes often caused grid-iron patterns to occur on the bed. However, if oblique crests are formed, then the antidunes disappeared (Fig. 5-8). From these experimental facts, the assumption made in Chapter 5-1, that rhomboid bars are formed by the combination of longitudinal striations and antidunes, is thought to be correct.

Fig. 5-9 shows the relationship between β and $\tan^{-1}(L_l/L_t)$ in runs where the three values, the spacing of longitudinal striations L_l, the wavelength of the antidunes L_t, and the angle between the rhomboid bar crests and flume side walls β, were all determined. The correspondence between the two values, β and $\tan^{-1}(L_l/L_t)$, is very close.

From Eq. (5-2), by substituting $2D$ for L_l, the following equation is obtained:

$$\beta = \tan^{-1}\frac{2D}{L_t} \quad \cdots\cdots\cdots\cdots\cdots\cdots\cdots\cdots\cdots\cdots \quad (5\text{-}4)$$

and this shows the relationship between β and $\tan^{-1}(2D/L_t)$ (Fig. 5-10). The correspondence between these two values is also very close.

Assuming that the wavelength of antidunes can be expressed by Eq. (5-2), the following equation can be obtained.

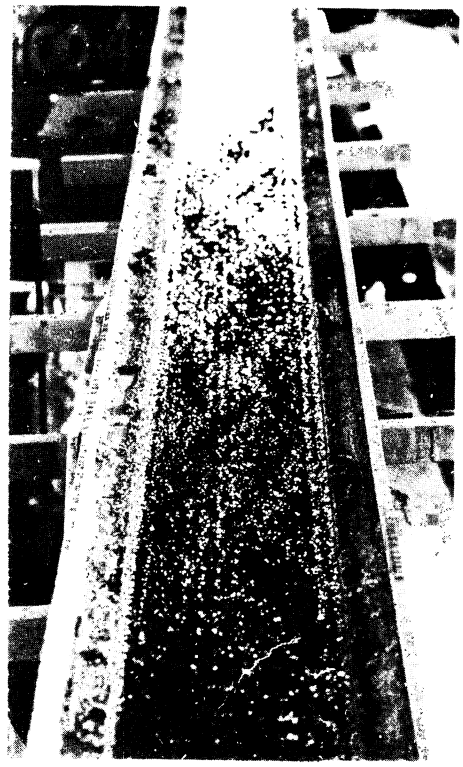

Fig. 5-7 Upstream view of grid-iron pattern for Run 101 (S = 1/100, D = 0.8 cm)

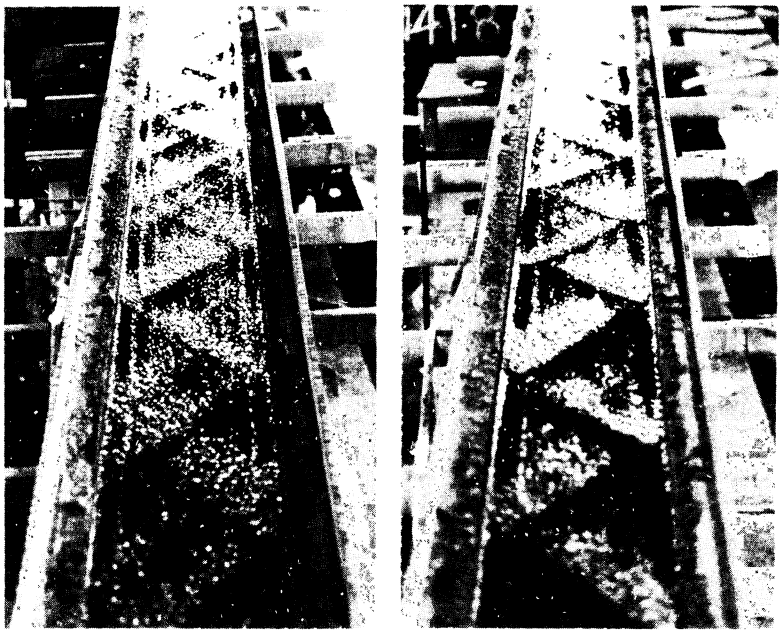

Fig. 5-8 Upstream views of diagonal bars and longitudinal striations
(A) Run 102, $S = 1/100$, $D = 1.2$ cm
(B) Run 142, $S = 1/140$, $D = 1.6$ cm
As the flow continues, rhomboid bars immediately merge into larger rhomboid bars.

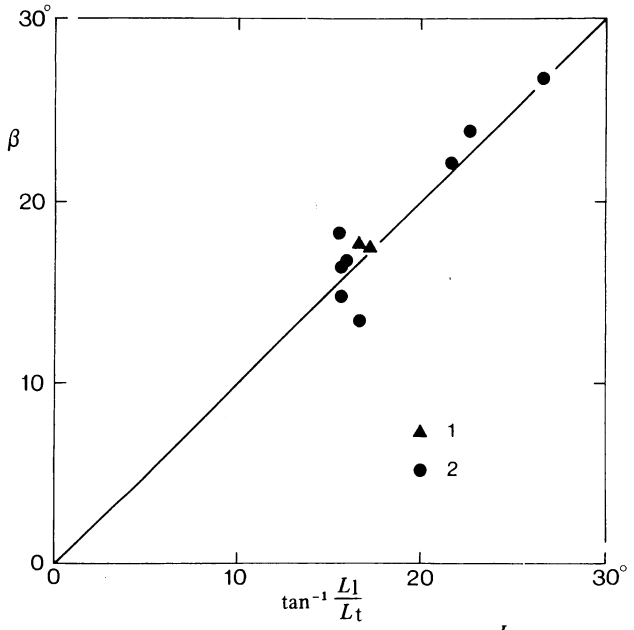

Fig. 5-9 Relationship between β and $\tan^{-1}\frac{L_l}{L_t}$
1: the 4-meter-wide flume,
2: the 0.2-meter-wide flume

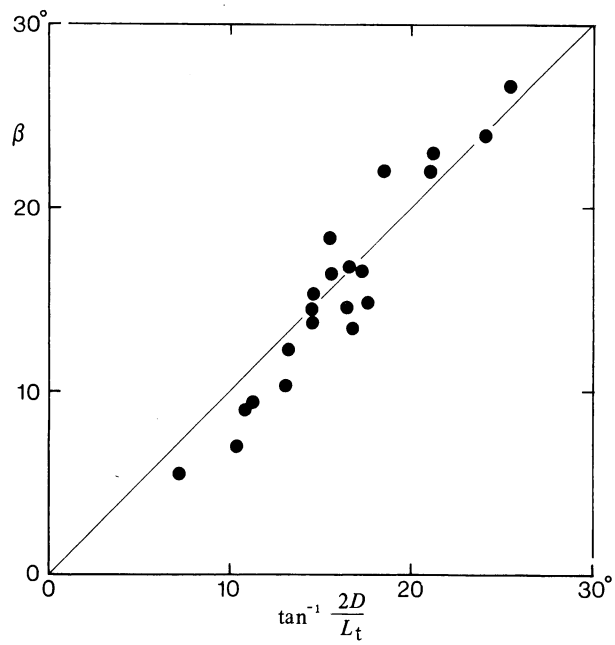

Fig. 5-10 Relationship between β and $\tan^{-1}\frac{2D}{L_t}$ in the 0.2 meter wide flume

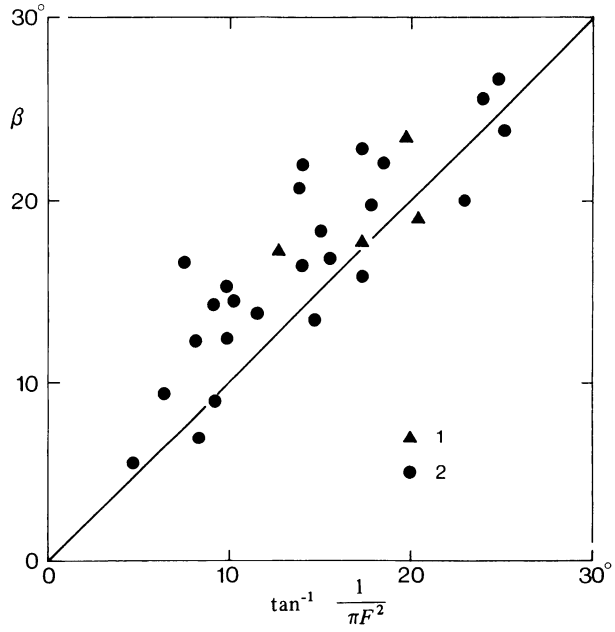

Fig. 5-11 Relationship between measured values of β and Froude number F
1: the 4-meter-wide flume
2: the 0.2-meter-wide flume

$$\beta = \tan^{-1}\frac{L_l}{L_t} = \tan^{-1}\frac{2D}{\frac{2\pi}{g}\cdot V^2}$$

$$= \tan^{-1}\frac{1}{\pi F^2} \qquad (5\text{-}5)$$

where, F : Froude number.

The relationship between the experimental values of β and the Froude number is shown in Fig. 5-11. One can say that there is a close relationship between β and the Froude number: β becomes smaller as the Froude number becomes larger. From this, the hypothesis that rhomboid bars are formed by the combination of longitudinal striations and antidunes, can be said to be correct, quantitatively, also. When the longitudinal elements on the bed are strong, longitudinal striations are formed, and when the transverse elements are strong, antidunes are formed. However, when the longitudinal and transverse elements are combined, rhomboid bars occur.

The formation of rhomboid bars on the bed is not due to the shock waves from the flume side walls. Rhomboid bars occur even under ordinary, or subcritical flow conditions (Kinoshita, 1961). Furthermore, the angle between the flume side wall and the shock waves from it, which ranged between 30° and 50° in this small flume experiment, did not agree with the angle made by the oblique crests.

As the water begins to flow, rhomboid bars form on the planed bed, despite the type of stable bedstate. Therefore, the condition for the formation of rhomboid bars is a shallow flow, which causes standing waves, occuring for a short period on a plane bed.

CHAPTER 6

SIMILITUDE LAW OF ALTERNATING BARS

Similitude law of alternating bars using the alternating bars experiment in the 4-meter-wide flume as a prototype, a model experiment was done, using a flume with a width 1/20th of the 4-meter-wide flume, and the similitude law of alternating bars was investigated (Ikeda, 1982 b).

6-1 Alternating bars formed in the 4-meter-wide flume

Runs 80 and 81 in Case 4, in Chapter 3-4, were chosen as prototypes. The change in position with time of the alternating bars of the prototypes are shown in Fig. 6-1, with change in position as the ordinate, and time as the abscissa.

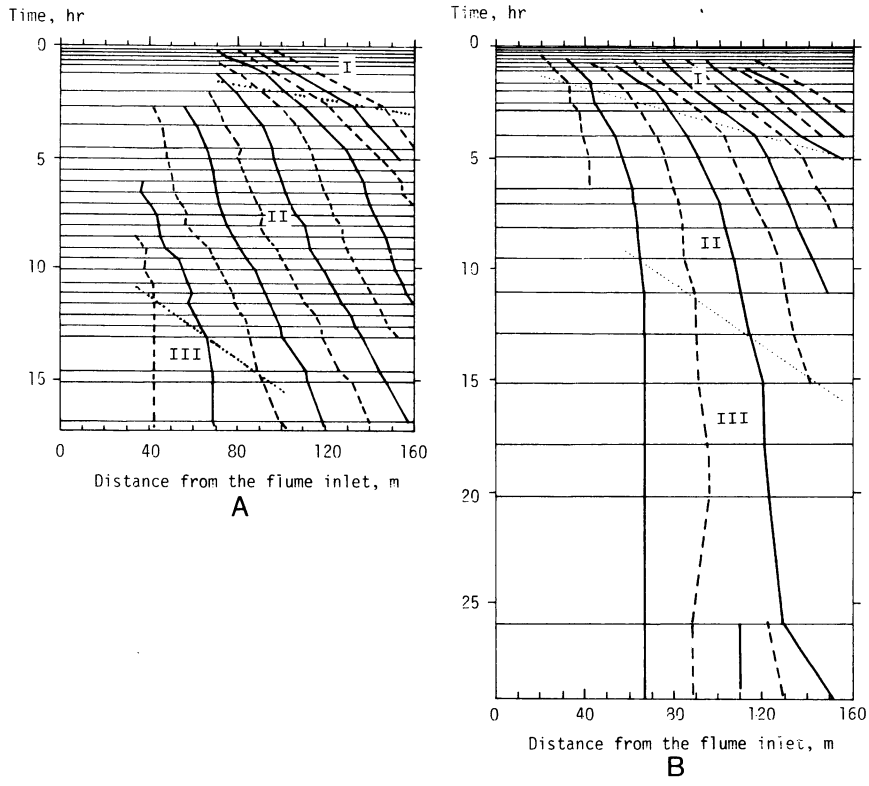

Fig. 6-1 Change in time of position of the alternating bars
(A) Run 80, $S = 1/100$, $Q = 0.4$ m^3/sec, $D = 10$ cm
(B) Run 81, $S = 1/100$, $Q = 0.35$ m^3/sec, $D = 9$ cm
Solid lines indicate the positions of alternating bar crests in contact with the left side wall. Broken lines indicate the opposite side.
I, II, and III are subphases of alternating bars.

For the convenience of discussion, I have divided the bar development process into three subphases, based on the progressive stages of bar development from an initially flat bed.

Subphase I : the stage in which the rhomboid bars develop into fast-moving, short wavelength, alternating bars.

Subphase II : the stage in which the wavelengths of the alternating bars gradually increase in length, and the migration velocity decreases.

Subphase III : the stage in which portions of the alternating bar crests emerge onto the water surface; in other words, sand banks are formed, and here, the migration velocity is extremely slow.

Some types of alternating bars are sketches in Fig. 6-2. The alternating bars formed in the prototype, Runs 80 and 81, correspond to the transitional form between double row bars and single row bars.

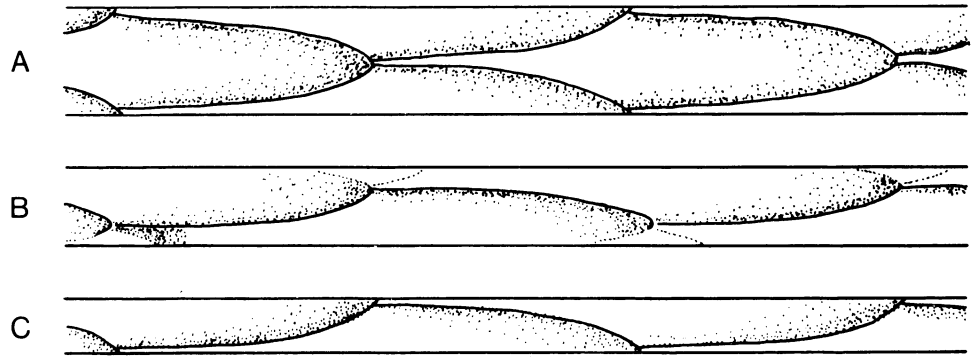

Fig. 6-2 Sketches of bar-types
(A) Double row bars, the most simple type of multiple row bars
(B) Transitional type of single to double row bars
(C) Single row bars, or alternating bars

6-2 Froude model experiments using 0.34 mm sand

Using the large flume experiments of Runs 80 and 81 as the prototype, a Froude model was made so that the Froude number ratio, F_r, between the prototype and the model, was 1, and several experiments were made, with slight variations in depth and slope (Table 6-1, F-1 ~ 9).

In the remainder of this paper, for any variable X, the value of the prototype will be referred to as X_p, that of the model as X_m, and the ratio between the two, X_p/X_m as X_r.

Here, the ratio between the length of the prototype and the model, L_r, was chosen to be 20, and a flume 20 cm wide and 8 m long, was used. Because the diameter of the bed material used in the prototype experiment was 5–10 mm, medium sand, with a diameter 1/20th of that of the prototype, 0.25–0.5 mm, was used in this experiment. The median sieve diameter was 0.34 mm.

In the Froude model, assuming that the ratio of the flow velocity in a horizontal direction, V_r, is given by $V_r = (L/T)_r$, the ratio of the Froude number, F_r, will be shown as the following:

$$F_r = \frac{V_r}{\sqrt{g_r D_r}} = \frac{L_r}{T_r \sqrt{L_r}} = \frac{\sqrt{L_r}}{T_r} = 1 \quad \cdots\cdots\cdots\cdots\cdots\cdots \quad (6\text{-}1)$$

Table 6-1 Summary of experimental data on similitude law of alternating bars

Run No.	W cm	L m	d_{50} mm	S	Q l/sec	T_w °C	V cm/sec	D cm	F	U_* cm/sec	W/D	D/d_{50}	U_*/U_{*c}	$S \cdot W/D$	Bed state	I_b g/sec
80	400	160	6.4	1/96	402	20	97	10.4	0.96	10.3	39	16	1.4	0.40	C	–
81	〃	〃	〃	1/96	352	15	100	8.8	1.07	9.4	45	14	1.3	0.46	B	450
F-1	20	8	0.34	1/100	0.208	〃	31	0.31	1.68	1.8	59	10	1.1	0.59	F	–
-2	〃	〃	〃	〃	0.194	〃	24	0.40	1.22	2.0	50	12	1.2	0.50	B	–
-3	〃	〃	〃	〃	0.212	〃	24	0.45	1.12	2.1	44	13	1.3	0.44	B	0.25
-4	〃	〃	〃	〃	0.264	〃	26	0.51	1.16	2.2	39	15	1.4	0.40	F～R	–
-5	〃	〃	〃	〃	0.353	14	26	0.67	1.03	2.6	30	20	1.6	0.30	R	–
-6	〃	〃	〃	〃	0.542	〃	33	0.81	1.19	2.8	25	24	1.7	0.25	R	–
-7	〃	〃	〃	1/50	0.153	〃	29	0.26	1.84	2.3	77	7.6	1.4	1.5	A	–
-8	〃	〃	〃	1/200	0.437	〃	26	0.84	0.63	2.0	24	25	1.3	0.12	R	–
-9	〃	〃	〃	〃	0.494	〃	21	1.16	0.91	2.4	17	34	1.5	0.09	R	–
D-1	〃	〃	0.81	1/50	0.246	15	26	0.48	1.18	3.1	42	6	1.5	0.83	A	–
-2	〃	〃	〃	1/76	0.346	〃	26	0.68	1.03	3.0	30	8	1.4	0.40	B	–
-3	〃	〃	〃	1/100	0.567	〃	32	0.90	1.06	3.0	22	11	1.4	0.22	C	–
-4	〃	〃	〃	1/76	0.356	14	29	0.61	1.19	2.8	33	7.5	1.3	0.43	B	0.39～0.55

Bed state:
A, double row bars; B, transitional form of A and C; C, typical alternating bars;
R, ripples; P, plane bed
– : not measured

Here, V : the flow velocity in a horizontal direction
D : water depth
L : length
g : gravity constant
T : time.

The ratio of the amount of discharge, Q_r, would be:

$$Q_r = L_r^3 \cdot T_r^{-1} = L_r^{5/2} \quad \cdots\cdots\cdots\cdots\cdots\cdots\cdots\cdots\cdots\cdots (6\text{-}2)$$

Hence, assuming $L_r = 20$ from the prototype's amount of discharge, 402 and 352 ℓ/sec, the amount of discharge of the model becomes 225 and 200 cc/sec.

The results of the Froude model experiment with a discharge of 212 cc/sec are shown in Fig. 6-3. Here, because fine grained sand was used, the bed form became rippled and was not similar to that of the prototype.

Fig. 6-3 Plan view of ripple bed for Run F-3 (S = 1/100, d_{50} = 0.34 mm, Q = 212 cc/sec, D = 0.45 cm)

6-3- Experiments using a distorted model

a) Similitude law for a distorted model

In order to avoid the occurence of ripples, coarse grained sand can be used as the bed material. However, in order to do this, distortion of the model will be necessary. Inokuchi and Sukegawa (1967) and Sukegawa (1972) first suggested the similitude law of a distorted model on the formation of alternating bar.

In analyzing the formation of alternating bars, Ikeda (1973) took into account Sukegawa's suggestion and assumed that, the flows in geometrically similar channels are similar when they have the same ratio of U_*/U_{*c}, in which U_* is the shear velocity of the flow and U_{*c} is the value of U_* for which the motion of the bed material is initiated. Thus,

$$(U_*/U_{*c})_r = 1 \quad \cdots\cdots\cdots\cdots\cdots\cdots\cdots\cdots\cdots\cdots \quad (6\text{-}3)$$

Also, from

$$g_r = 1$$

he obtained the following:

$$(U_*/U_{*c})_r = (\sqrt{gDS}/U_{*c})_r = \sqrt{g_r \cdot Y_r \cdot \frac{Y_r}{L_r} \cdot \frac{1}{U_{*cr}}}$$

$$= \frac{Y_r}{\sqrt{L_r}} \cdot \frac{1}{U_{*cr}} = 1 \quad \cdots\cdots\cdots\cdots\cdots\cdots \quad (6\text{-}4)$$

where, g : gravitational constant
D : water depth
Y : scale of vertical direction
L : scale of horizontal direction.

Therefore, the ratio of the slope S, S_r, is:

$$S_r = \frac{Y_r}{L_r} = U_{*cr} \cdot \frac{1}{\sqrt{L_r}} \quad \cdots\cdots\cdots\cdots\cdots\cdots\cdots\cdots \quad (6\text{-}5)$$

and here, by substituting the ratio of the flume width W, W_r, for L_r in Eq. (6-5), we obtain:

$$\frac{S_r \cdot W_r^{1/2}}{U_{*cr}} = \left(\frac{U_*}{U_{*c}}\right)_r \cdot \left(\frac{S \cdot W}{D}\right)_r^{1/2} = 1 \quad \cdots\cdots\cdots\cdots \quad (6\text{-}6)$$

As $(U_*/U_{*c})_r = 1$, the following equation can be derived as the model rules for the model to become similar to the prototype.

$$(S \cdot W/D)_r = 1 \quad \cdots\cdots\cdots\cdots\cdots\cdots\cdots\cdots\cdots\cdots \quad (6\text{-}7)$$

Ikeda (1973) called $S \cdot W/D$, the channel-form index.

Furthermore, Ikeda (1975) made it clear that when considering bed configurations in natural

river channels, the values of the hydraulic variables at a bankfull stage could be used.

b) Distorted model experiments using 0.81 mm sand

In order to prevent the occurence of ripples, uniform, coarse sand – median grain size: 0.81 mm; critical shear velocity U_{*c}: 2.1 cm/sec, were used for the bed material. The length ratio, L_r, was 20, the same as that in the Froude model experiments. The prototype bed material had a median grain size of 6.4 mm and because the U_{*c} was 7.2 cm/sec, $(U_{*c})_r = 7.2/2.1 = 3.4$. From $(U_*/U_{*c})_r = 1$, it was necessary for the value of U_{*r} to be established at $U_{*r} = 3.4$. Because $U_{*r} = (Y_r \cdot \frac{Y_r}{L_r})^{1/2}$, substituting $L_r = 20$, $Y_r = 3.4\sqrt{L_r} = 15.3$, was obtained.

Therefore, as the depth of the prototype, D_p, was 10.4 and 8.8 cm, the depth of the model, D_m, was calculated to be 0.68 and 0.58 cm. Because the slope ratio, $S_r = Y_r/L_r$, the slope of the model, S_m, can be given by $S_m = S_p \cdot L_r/Y_r$. Also, since the prototype slope, $S_p = 1/100$ and $L_r/Y_r = 20/15.3 = 1.3$, the model slope, S_m, will be $S_m = 1/77$.

Furthermore, assuming the area of the flow cross section to be A, the ratio of the amount of discharge, Q_r, is given by

$$Q_r = V_r \cdot A_r = \frac{L_r}{T_r} \cdot Y_r \cdot L_r = \frac{L_r^2 \cdot Y_r}{T_r} \quad \cdots\cdots\cdots\cdots \quad (6\text{-}8)$$

Because the ratio of the Froude number is

$$F_r = \frac{V_r}{\sqrt{Y_r}} = \frac{L_r}{T_r} \cdot \frac{1}{\sqrt{Y_r}} = 1 \quad \cdots\cdots\cdots\cdots\cdots\cdots\cdots\cdots \quad (6\text{-}9)$$

T_r will be,

$$T_r = L_r \cdot \frac{1}{\sqrt{Y_r}} = 5.7 \quad \cdots\cdots\cdots\cdots\cdots\cdots\cdots\cdots \quad (6\text{-}10)$$

Substituting Eq. (6-10) into Eq. (6-8), then,

$$Q_r = L_r \cdot Y_r^{3/2} = 1200 \quad \cdots\cdots\cdots\cdots\cdots\cdots\cdots\cdots \quad (6\text{-}11)$$

Hence, the amount of discharge of the model, Q_m, will be 336 and 294 cc/sec. Furthermore, the flow velocity ratio, V_r, will be given by

$$V_r = \frac{L_r}{T_r} = \sqrt{Y_r} = 3.9 \quad \cdots\cdots\cdots\cdots\cdots\cdots\cdots\cdots \quad (6\text{-}12)$$

The experiments were carried out from the calculated values obtained for the experimental conditions. As a result, the formation of the alternating bars extremely similar to those of the prototype were obtained (Fig. 6-4B). However, when using different experimental values, the shape of the alternating bars differed clearly with that of the prototype (Figs. 6-4A and 6-4C).

The change in position of the alternating bars in Run D-4 is shown in Fig. 6-5. This is quite similar to that of the prototype, Fig. 6-1, and can be divided into 3 subphases. The length of the alternating bars and the migration velocity of each subphase were compared (Table 6-2). It can be said that, in subphase II, the values for the length and velocity of the alternating bars in the model and the prototype were nearly the same.

Furthermore, the model's mean velocity, V_m, was 26 cm/sec and 29 cm/sec and $V_r = 3.9$,

LIST OF FIGURES

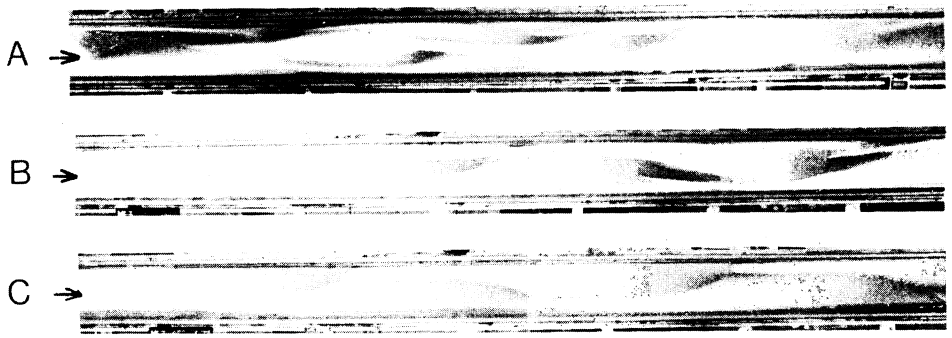

Fig. 6-4 Plan view of bars in the 0.2-meter-wide flume
(A) Run D-1, S = 1/50, Q = 246 cc/sec, bed state = double row bars
(B) Run D-4, S = 1/76, Q = 356 cc/sec, bed state = similar to prototype (Run 80 and 81)
(C) Run D-3, S = 1/100, Q = 567 cc/sec, bed state = typical alternating bars

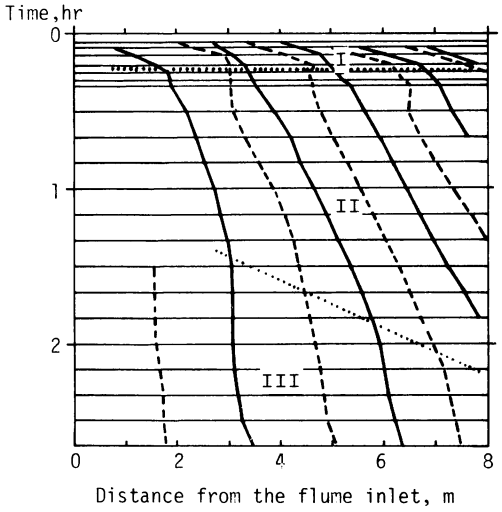

Fig. 6-5 Change in time of position of alternating bars for Run D-4 (S = 1/76, Q = 356 cc/sec)
I, II, and III are the subphases of alternating bars.

Table 6-2 Comparison of experimental results of Run D-4 with values of Run 80 and 81

	Prototype				Model		
	Run 80		Run 81		Run D-4		
Subphase	$(\lambda/W)_p$	V_{bp} m/hr	$(\lambda/W)_p$	V_{bp} m/hr	$(\lambda/W)_m$	V_{bm} m/hr	V_{bm}/V_r m/hr
I	2.3	18.8	2.4	12.9	3.4	11.0	43.1
II-1	2.8	9.4	3.9	4.6	4.5	1.5	5.9
II-2	4.2	4.2	5.0	2.4	6.1	0.6	2.3
III	6.1	0	6.6	0	7.5	0	0

λ, length of alternating bars; W, flume width; V_b, migration velocity of alternating bars

thus, V_p = 102 cm/sec and 113 cm/sec, which are nearly the same as the mean velocity of the prototype, 1 m/sec.

This experiment confirmed that, by making the flow intensity, U_*/U_{*c}, and the size of the channel form index, $S \cdot W/D$, equal to that of the prototype, the bed configuration of the model would become similar to the prototype. Hence, the similitude law (or model rules) of alternating bars can be expressed by the following equation:

$$(U_*/U_{*c})_r = (S \cdot W/D)_r = 1 \quad \text{(6-13)}$$

CHAPTER 7

OPENWORK GRAVEL LAYERS

7-1 Openwork gravel layers formed in the 4-meter-wide flume experiments

Gravel layers in natural alluvial channels are commonly filled with matrices of sand and silt. In some fluvial deposits, however, there are "openwork gravel layers", i.e., gravel layers without matrices.

Because the fine gravel used in the 4-meter-wide flume experiments was originally sorted artificially, it contained very little sand, and naturally, there were only openwork gravel layers at the beginning of the experiment. However, after recirculating the fine gravel in the flume system for a long period, a small amount of sand was obtained due to the abrasion of the fine gravel. It was observed that the sand was not distributed uniformly in the bed material but rather that it was distributed unevenly, and that this was closely related to the bed form.

Fig. 7-1 shows the low relief dunes seen from the upstream in the 4-meter-wide flume, where the slope was set at 1/400, and the discharge at 1 m^3/sec. By dyeing the surface gravel of several dunes, and allowing water to flow into the flume, the movement of the dyed gravel was investigated. The results showed that the dunes, under these conditions, changed position while maintaining their shape. In other words, the movement of the gravel composing the dunes resembled that of a caterpillar (Fig. 7-2).

In this experiment, whereas the crests of the dunes were openwork gravel layers, the troughs of the dunes were matrix-filled gravel layers with san filling the pores among the gravel particles (Fig. 7-3).

Fig. 7-1 Downstream view of low-relief dunes formed in the 4-meter-wide flume (S = 1/400, Q = 1 m^3/sec)

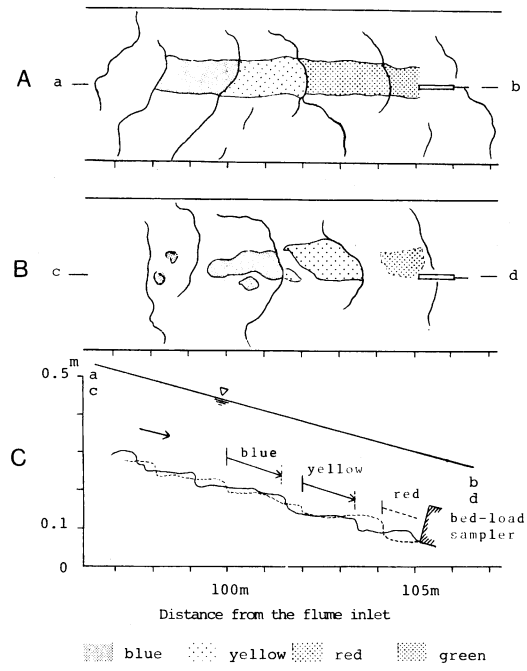

Fig. 7-2 Migration of dunes (S = 1/400, Q = 1 m^3/sec)
(A) Before start of run
(B) 5 minutes after start of run
(C) Bed surface profiles; broken lines indicate (A), solid lines indicate (B)

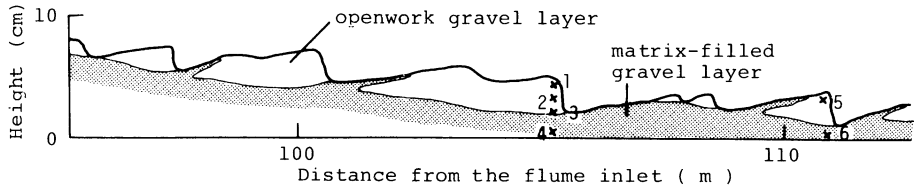

Fig. 7-3 Internal structure of low-relief dunes (S = 1/100, Q = 1 m^3/sec)
The x's are sampling points of bed material. Grain size distributions of them are shown in Fig. 7-4.

7-2 Experiments on the transport of the sand and gravel mixture

Ikeda (9182 a), in his flume experiments, investigated the conditions for the formation of openwork gravel layers, resulting from the segregation of gravel and sand due to water flow. The recirculating flume, made from clear plastic, was 9 m long, 0.3 m wide, and 0.3 m deep. Fine black gravel and fine white sand were used as bed material (Table 7-1).

Two cases were provided as experimental conditions.
Thus,

Case A: condition of upper flow regime
Case B: condition of lower flow regime.

In each case, the discharge and the slope were kept as constant as possible, and the sand con-

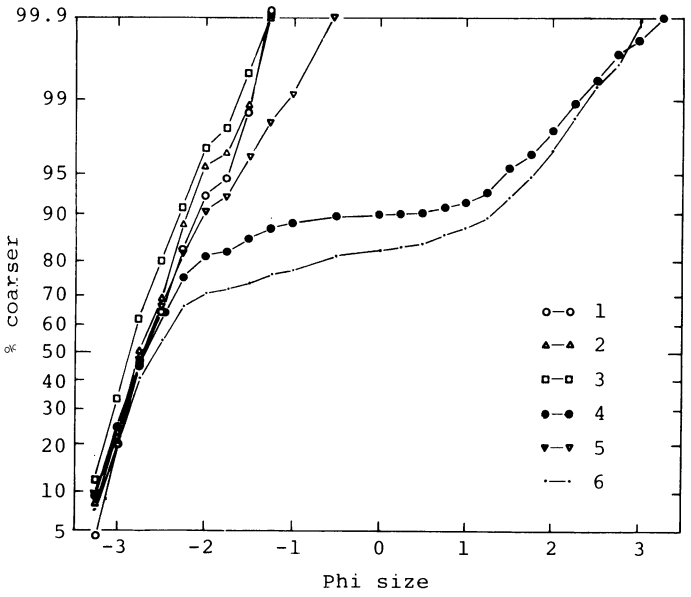

Fig. 7-4 Log probability plots showing grain size distribution of openwork gravel layers and matrix-filled gravel layers
Sampling points are shown in Fig. 7-3.

Table 7-1 Properties of sand and gravel used

	d_{50}, mm	S_o	σ/ρ	porosity, %
Gravel	4.3	0.27	2.6	40
Sand	0.20	0.20	2.6	41

d_{50} = median diameter, σ = density of solid particles,
$S_o = (\phi_{84} - \phi_{16})/2$, ρ = density of water

tent of the bed material was varied in stages (Table 7-2). How the concentration of the sediment discharge and the sand content of the sediment discharge of Cases A and B change with an increase in the sand content of the bed material, is shown in Fig. 7-5. The change in bedform and sedimentary structures is schematically shown in the same figure.

Case A consisted entirely of a plane bedform in the upper flow regime. It is a matter of course that an openwork gravel layer was formed when the bed material was made up of gravel only. As sand grains were added to the flume system, the grains fell down through the interstices of the gravel layer to the fixed bottom of the flume, and filled the pores near the fixed bottom to make a matrix-filled gravel layer (Fig. 7-6). The phenomenon that small particles filling pores in a gravel layer hide from the flow, the hiding effect, has already been noted by Einstein and Chien (1953). It was also observed that, the higher the sand content of the bed material was, the thicker the matrix-filled layer became. The upper openwork gravel layer decreased gradually in thickness.

Just when the pores among the gravel particles were entirely filled with sand grains, the

Table 7-2 Experimental conditions and results on transport of sand and gravel mixture

Run No.	M %	S %	Q l/sec	T_w °C	V_s cm/sec	D cm	V cm/sec	Bed State	C_t g/l	C_s/C_t %
A – 2	18.1	3.36	11.1	11.5	119	3.20	116	P	17.5	0.00
6	20.5	3.34	10.7	12.5	117	3.72	95.9	P	17.0	0.25
8	21.8	3.36	9.35	12.2	116	3.05	102	P	15.5	0.87
10	22.3	3.29	10.3	10.2	116	2.90	118	P	23.8	22.3
12	28.9	3.26	10.3	15.1	118	3.05	113	A ~ P	25.5	32.7
17	33.0	3.52	10.6	–	120	3.11	114	A ~ P	47.8	47.7
B – 1	0.0	3.36	4.11	12.0	72.8	1.92	71.4	B	–	0.00
3	18.1	3.32	4.58	13.0	78.4	1.82	83.9	B	13.3	1.90
7	20.5	3.40	3.74	15.2	73.9	1.82	68.5	B	14.5	15.1
9	21.8	3.36	3.93	14.0	75.6	2.13	61.5	B	14.2	18.3
11	22.3	3.49	4.21	15.0	73.0	1.95	72.0	B	14.2	33.3
16	28.6	3.29	3.65	14.0	82.8	1.71	71.2	B	14.0	39.6

Bed state:
A, antidunes; B, bars; P, plane bed
– : not measured

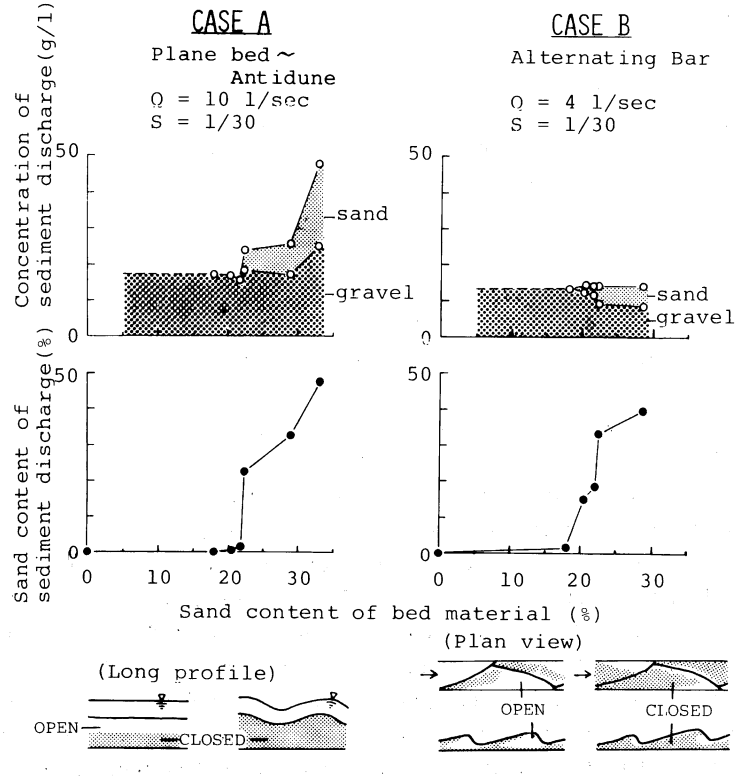

Fig. 7-5 Influence of sand content of bed material on transport and deposition of sand and gravel mixture

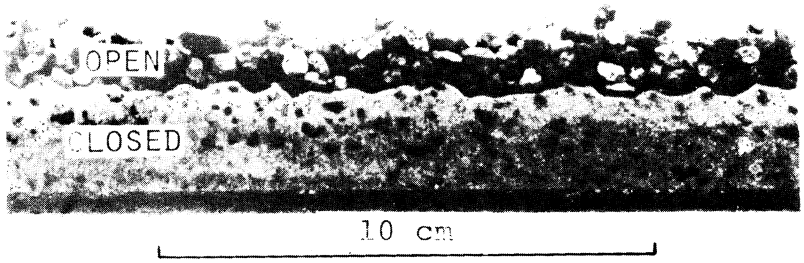

Fig. 7-6 Openwork gravel layers and matrix-filled gravel layers formed during Run A-8

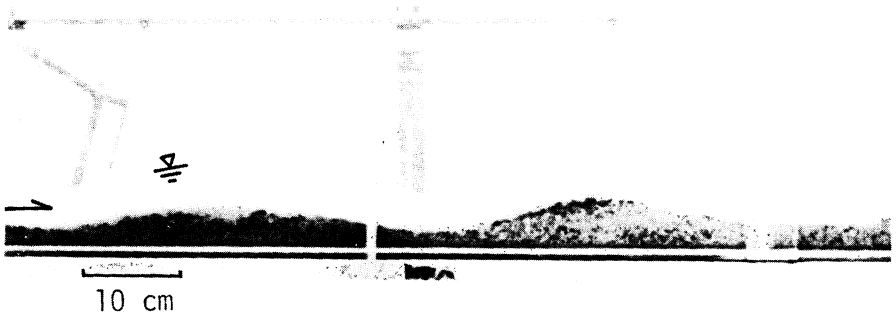

Fig. 7-7 Antidunes of Run A-17
No segregation of sand from gravel occur in the bed material.

bed form changed abruptly from the plane bed to antidunes (Fig. 7-7). Under this flow condition, some of the sand grains were carried in suspension, but most were shielded from the flow by the presence of gravel near the bed surface and were carried with the gravel as a traction load. In such a situation, no segregation of sand from the gravel layer occurred on the bed surface, and the openwork gravel layer was never formed.

Case B showed that the bed configuration consisted of alternating bars and that the size distribution of the bed material depended largely on the position of the surface on a single bar. In the case of low content of sand in the bed material, most of the sand grains were trapped by the gravel on the stoss slope of the bar, and were unable to reach the crestal part of the bar (Fig. 7-8). Hence, the openwork gravel layers remained only in the bar crest area. The migration and accumulation of a single bar or a dune, made a pair of openwork and matrix-filled gravel layers. On the other hand, when the sand content of the bed material increased, all of the pores, even in the openwork gravel layers on the bar crest, were finally filled with sand grains.

7-3 Conditions for the formation of openwork gravel layers

Smith (1974) investigated the bar formation and sediment distribution patterns in a gravel bedded channel and noted that some bars contained alternation of thin openwork gravel layers

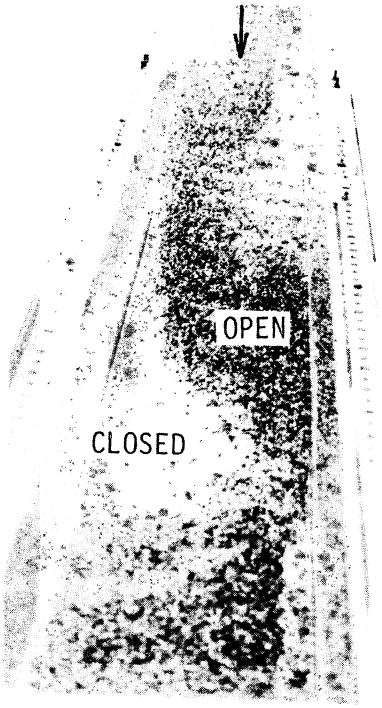

Fig. 7-8 Upstream view of alternating bar-bed configuration for Run B-16
Matrix-filled gravel appears to be white.

and matrix-filled layers in a cyclical fashion. Smith thought that these open-closedwork gravel alternations arose from normal discharge fluctuations. In other words, he thought that the openwork gravel was deposited during the high flow, when most of the fines were carried in suspension. He also thought that, as the flow diminished, the suspended grains settled into pores and were trapped by the surface layer, thus forming matrix-filled layers.

I would like to add a new evidence of the formation of openwork gravel layers from my experimental results of Case A described in the previous Section 7-2.

A part of the sand becomes trapped by the presence of gravel at the bed and withstands removal by a high flow. This happens even when there is a high flow condition in the upper flow regime where the gravel is transported as the bed load and most of the sand is also transported in suspension. Sand remains in the pores of gravel, thus, causing the matrix-filled gravel layers to form, but not the openwork gravel layers.

The experimental results of Case A and Case B showed that when the sand content of the bed material is very small, it is quite natural for the openwork gravel layers to form. This idea is supported by the field observations, that openwork gravel layers are sometimes found along rivers in which their mountainous areas are composed of rocks (for example, sedimentary rocks such as chert or slate), which will produce little sand. However, in general, even when the sand content of the bed material is large, openwork gravel layers may also be formed.

As shown from the experimental results of Case B, the reason for this is that when the bed form is formed, the bed material is sorted, and bed material with different grain sizes have dif-

ferent migration velocities and modes. In other words, because the bed material is segregated and migrates differently according to grain size, if, during the deposition of the gravel, no sand migrates, an openwork gravel layer is formed. In order to understand the origin of sedimentary structures, further research on the sorting process of non-uniform sediments due to water flow, is desired.

ACKNOWLEDGEMENTS

Dr. Masao Inokuchi, the former Directer of the Environmental Research Center, the University of Tsukuba, initially motivated me to conduct the present study, and has subsequently followed it with great interest throughout all its phases. He has read through the entire manuscript and made many valuable comments. Dr. R. Kinoshita, Jiyugakuen Colledge, has given many helpful suggestions during these flume experiments. Many colleagues at the Environmental Research Center assisted in various ways to complete the present experimental study. Among those, I would especially like to thank Mr. H. Kojima for making several small flumes and useful equipment. Mrs. T. Kai and many students have helped me to carry out the experiments. In particular, the assistance given by Miss F. Iseya has been valuable. She has arranged the flume data and has drawn the figures. English wording and typing of the manuscript are due to Miss Y. Doi and Miss N. Tanaka. I have been strongly encouraged by Dr. M. M. Yoshino, Directer of the Environmental Research Center, on the publication of this paper. He has also read through the manuscript and made many valuable comments. For all the persons and institutions, even those not mentioned here by name, who have helped in the completion of this work, I wish to express my sincere thanks.

REFERENCES

Allen, J.R.L. (1968): *Current ripples : their relation to patterns of water and sediment motion.* North-Holland, Amsterdam, 433p.

Bagnold, R.A. (1960): Sediment discharge and stream power, a preliminary announcement. *U.S. Goelogical Survey Circular,* **421**, 23p.

Bagnold, R.A. (1966): An approach to sediment transport problem from general physics. *U.S. Geological Survey Prof. Paper,* **422-I**, 37p.

Bagnold, R.A. (1973): The nature of saltation and of bed-load transportation in water. *Proc. Roy. Soc. London, Ser. A,* **332**, 473-504.

Bagnold, R.A. (1977): Bed load transport by natural rivers. *Water Resources Research,* **13**, 302-312.

Einstein, H.A. and Chien, N. (1953): Transport of sediment mixtures with large ranges of grain sizes. *Berkeley, Calif., Univ. California, Inst. Engineering Research,* 49p.

Graf, W.H. (1971): *Hydraulics of sediment transport.* McGraw-Hill, New York, 513p.

Griffith, W.M. (1927): A theory of silt and scour. *Proc. Inst. Civil Eng.,* **223**, 243-314.

Guy, H.P., Simons, D.B. and Richardson, E.V. (1966): Summary of alluvial channel data from flume experiments, 1956-61. *U.S. Geological Survey Prof. Paper,* **462-I**, 96p.

Ikeda, H. (1973): A study on the formation of sand bars in an experimental flume. *Geographical Review of Japan,* **46**, 435-451. (in Japanese with English abstract)

Ikeda, H. (1975): On the bed configration in alluvial channels: their types and condition of formation with reference to bars. *Geographical Review of Japan,* **48**, 712-730. (in Japanese with English abstract)

Ikeda, H. (1978): Width effects on bed-load transport rate in constant discharge flume. *Bull. Environ. Res. Center (Univ. of Tsukuba),* **2**, 1-7. (in Japanese)

Ikeda, H. and Inokuchi, M. (1979): Effects of water depth and slope on sediment transport. *Bull. Environ. Res. Center (Univ. of Tsukuba),* **3**, 1-5. (in Japanese)

Ikeda, H., Ono, Y., Izumi, K. and Kawamata, R. (1979): The speeds of solid grains, rolling allong the smooth bed. *Bull. Environ. Res. Center (Univ. of Tsukuba),* **3**, 7-15. (in Japanese)

Ikeda, H. (1980): Experiments on the transport of fine gravel in 4-meter-wide flume. *24th Intern. Geographical Congress, Abstracts* **1**, 24-25.

Ikeda, H. (1981): Experiments on the transport of fine gravel in 4-meter-wide flume: effect of threshold stream power on sediment transport rate. *Bull. Environ. Res. Center (Univ. of Tsukuba),* **5**, 35-49. (in Japanese)

Ikeda, H. (1982a): An experimental study of the formation of openwork gravel layers under alluvial-flow conditions. *Trans. Japanese Geomorphological Union,* **3**(1), 57-65. (in Japanese with English abstract)

Ikeda, H. (1982b): Experimental study of the similitude law of alternating bars. *Bull. Environ. Res. Center (Univ. of Tsukuba),* **6**, 3-14. (in Japanese)

Inokuchi, M., Ikeda, H., Ono, Y., Izumi, K. and Kawamata, R. (1980): The 4-meter-wide flume in the Environmental Research Center. *Bull. Environ. Res. Center,* **4**, 55-87. (in Japanese)

Inokuchi, S. and Sukegawa, N. (1976): On the criteria of bed forms in alluvial channels: domain of alternating bar formation. *Proc. 11th Japanese Conference on Hydraulics,* **13-18.** (in Japanese)

Kennedy, J.F. (1961): Stationary waves and antidunes in alluvial channels. *Cal. Inst. Tech.: W.M. Keck Lab. Hydraulics Water Research Report,* KH-R-2.

Kennedy, J.F. (1963): The mechanics of dunes and antidunes on erodible-bed channels. *J. Fluid Mech.,* **16**, 521-544.

Kinoshita, R. (1961): Historical survey of meander for the Ishikari River. *Rept. Natural Resources Bureau (Science and Technology Agency)*, No. 36, 137p. (in Japanese)

Kinoshita, R. (1962): Historical survey of meander for the Ishikari River: Appendix. *Rept. Natural Resources Bureau (Science and Technology Agency)*, No. 36, 174p. (in Japanese)

Lane, E.W. (1937): Stable channels in erodible materials. *Trans. Am. Soc. Civil Eng.*, **102**, 123-142.

Nordin, C.F., Jr. (1964): Aspects of flow resistance and sediment transport, Rio Grande near Bernalillo, New Mexico. *U.S. Geological Survey Water Supply Paper*, **1498-H**, 41p.

Smith, N.D. (1974): Sedimentology and bar formation in the upper Kicking Horse River, a braided outwash stream. *J. Geol.*, **82**, 205-223.

Sukegawa, N. (1972): Hydraulic conditions for the formation of alternating bars in experimental flumes. *Proc. Jap. Soc. Civil Engrs.*, **207**, 47-60. (in Japanese)

Tanaka, Y. (1970): An experimental study on antidunes. *Disaster Prevention Res. Inst. (Kyoto Univ.) Annuals*, No. **12B**, 271-284. (in Japanese with English abstract)

Vanoni, V.A. (1975): River dynamics. *Advances in applied mechanics.* Academic Press, **15**, 1-87.

Vincent, J. (1967): Effect of bed-load movement on the roughness coefficient value. *Proc. I.A.H.R.*, **A 20**, 162-171.

Williams, G.P. (1970): Flume width and water depth effects in sediment transport experiments. *U.S. Geological Survey Prof. Paper*, **562-H**, 37p.

Wolman, M.G. and Brush, L.M., Jr. (1961): Facters controlling the size and shape of stream channels in coarse non-cohesive sands. *U.S. Geological Survey Prof. Paper*, **282-G**, 183-209.

Environmental Research Center Papers

No. 1 (1982) Kenji KAI : Statistical characteristics of turbulence and the budget of turbulent energy in the surface boundary layer. 54p.

No. 2 (1983) Hiroshi IKEDA : Experiments on bedload transport, bed forms, and sedimentary structures using fine gravel in the 4-meter-wide flume. 78p.

No. 3 (1983) Yousay HAYASHI : Aerodynamical properties of an air layer affected by vegetation. 46p.

発行　　昭和58年2月10日

編集・発行者　筑波大学水理実験センター

〒305 茨城県新治郡桜村天王台1－1－1

TEL 0298(53)2532, 2534

印刷　日青工業株式会社

東京都港区西新橋2－5－10